NONSTATIONARY SINUSOIDAL MODEL FREQUENCY PARAMETER ESTIMATION VIA FRESNEL INTEGRAL ANALYSIS

Report for JOS Review

Aaron S. Master

August 19, 2002

Abstract

In this report we show, via a Fresnel integral analysis, that linear frequency chirp functions have FFTs with parabolic phase in the FFT region corresponding to the frequencies contained in the signal. We begin with a brief review of Fresnel integrals, and then provide a theoretical discrete-time proof. We state all assumptions and approximations explicitly, and provide rigorous analysis of the error introduced by each assumption. We include examples showing that our model is invertible, and that it obtains estimates of the chirp parameter accurate to within 3% for cases where our assumptions are satisfied. We also mention and provide examples for alternative models for cases where our original assumptions are not satisfied.

Contents

1 Introduction

1.1 Objective and Overview

In conventional sinusoidal modeling parameter estimation [5, 4], peaks are treated as representative of quasistationary sinusoids. This is so even when such peaks are wider, which often indicates that the sinusoid[1] is changing in frequency. Herein, we seek to determine if the sinusoid is in fact linearly (or approximately linearly) changing in frequency, and if so, at what approximate rate. We then parameterize the sinusoid in terms of its amplitude, center frequency, and rate of linear frequency change.

In order to achieve our objective, we must first have an invertible model of a linear frequency chirp. To this end, we consider a linear chirp signal centered about DC and investigate its STFT phase characteristic. In order to perform this analysis, we see that an understanding of Fresnel integrals is required. Thus, a review is included in section 2. Equipped with this understanding, we proceed in section 3 to show that we may obtain invertible closed form approximations of the magnitude and phase of the STFT of a linear chirp signal. Doing so requires two nontrivial assumptions which are discussed as they are made. Next, in section 4, we invert the expressions formed in section 3 to obtain a method for extracting the frequency change parameter from an STFT peak. Finally, we demonstrate the performance of our algorithm in section 5.

We make an important note that the approximations used herein require significant constraints on the rate of frequency change. Thus, the method outlined in the body of this paper is not in general suitable for use on typical speech or music signals, whose frequency varies more slowly than signals used here. Modifications to the approach used here do, however, allow for such application. Alternative models allowing for this application are summarized in appendix A, and will be addressed in detail in an upcoming paper.

1.2 Previous Work

1.2.1 Nonstationary Sinusoidal Modeling

Previous work relevant to the current system falls into two general categories: nonstationary sinusoidal modeling parameter estimation and Fresnel analysis. The author included a review of the former in [3]. To summarize, previous work has focused on better matching sinusoidal trajectories across frames, rather than on trying to get better data at the frame level. The author's work ([3]), however, used a vocoder model at the frame level to better parameterize so-called smeared spectral peaks that tend to indicate nonstationary quasi-sinusoidal signals. In the process of creating the system presented therein, the author discovered that for practical speech and audio signals, the frequency trajectories were in general slowly varying enough to be well-modeled as linear. That observation is a motivating factor for the current system, which, in application, implicitly assumes that this is true.

Recent work by Liu [2] has investigated linear frequency chirps in continuous time, and has included a closed form expression for the frequency slope parameter as a function of the Fourier transform and its second derivative. This model, however, is more sensitive to noise than the currently proposed models, and loses accuracy for signals whose frequency changes only slowly. Modifications to Liu's model are being researched by the author.

1.2.2 Fresnel Analysis

The second major area of relevance, Fresnel analysis, appears to have gained little or no attention in the audio signal processing field. It has, however, seen many assorted applications in physics, and the approximation of Fresnel integrals has received much attention in mathematical and computational research. A more detailed review of such research is forthcoming.

2 Review of Fresnel Integrals

As suggested above, the current analysis is dependent on an understanding of Fresnel integrals. Thus, a brief review based on [6] is included here. Those familiar with the definitions, properties, and approximations of Fresnel integrals may wish to skip to the next section.

2.1 Definitions

We will use the definition[2] of Fresnel cosine and sine integrals oft seen in physics:

$$C(u) \equiv \int_0^u \cos\left(\frac{\pi}{2}x^2\right) \tag{1}$$

[1] The more accurate term here is "quasi-sinusoidal signal" though we use "sinusoid" for convenience.

[2] When we cast these integrals in a slightly different form [6], we may obtain exact solutions by infinite sums of spherical Bessel functions of the first kind.

$$S(u) \equiv \int_0^u \sin\left(\frac{\pi}{2}x^2\right) \tag{2}$$

2.2 Approximations

2.2.1 Large Limits Approximations

When cast as above and with $u \gg 1$, a two term asymptotic approximation may be used with great accuracy[3]. We aptly call this the large limits approximation.

$$C(u) \approx \frac{1}{2} + \frac{1}{\pi u}\sin\left(\frac{\pi}{2}u^2\right) \tag{3}$$

$$S(u) \approx \frac{1}{2} - \frac{1}{\pi u}\cos\left(\frac{\pi}{2}u^2\right) \tag{4}$$

In figure 1 below, we show $C(u)$ and $S(u)$, along with the large limits approximations in equations 3 and 4. For visual clarity, we plot these approximations (and their negative counterparts) for $|u| > 0$ even though they are intended to be valid only for $|u| \gg 1$.

In figure 2, we show the magnitude of the fractional errors resulting from use of the large limits approximation. We note that the two error functions are loosely anti-correlated, with larger errors corresponding to analogous portions of their 90°-out-of-phase sinusoids. Since the fractional error becomes infinite as u approaches zero, we show a zoom-in of the plot.

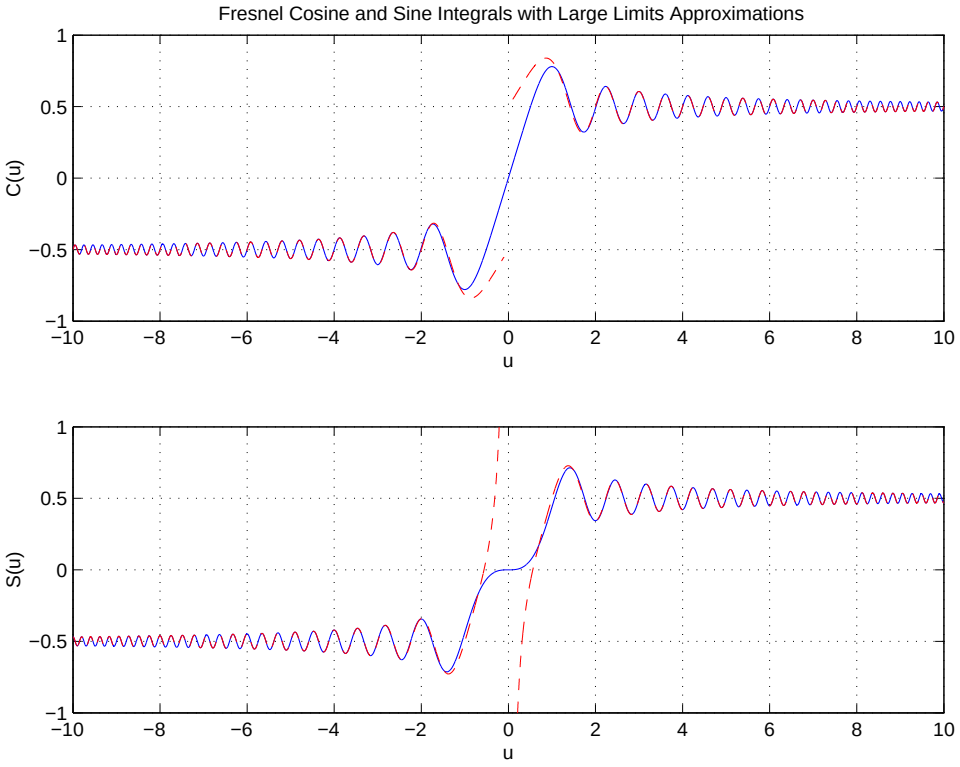

Figure 1: C(u) and S(u) (solid) with large limits approximations (dashed)

2.2.2 Infinite Limits Properties and Approximations

By observation of the above approximation for $C(u)$ and $S(u)$, we see that as u goes to infinity, the second term in each approximation goes to zero. Since both $C(u)$ and $S(u)$ are odd symmetric, we then have the following convenient facts:

$$C(\infty) = S(\infty) = \frac{1}{2} \tag{5}$$

[3] Efficient computation of numerical approximations of these sums has been a subject of mathematical research. In August of 2000, for example, Mielenz showed that a particular manipulation of the problem allowed an approximation accurate to within $5 * 10^{-10}$ as a sum of eleven precisely weighted terms.

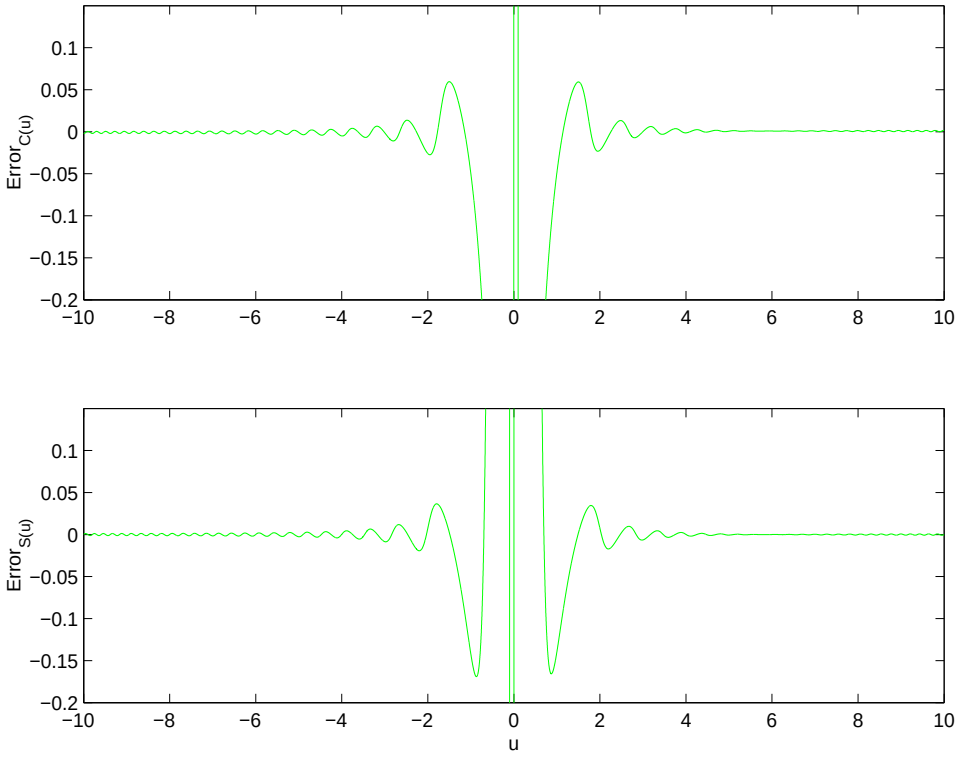

Figure 2: Fractional Errors in C(u) and S(u) resulting from the large limits approximations.

$$C(-\infty) = S(-\infty) = -\frac{1}{2} \tag{6}$$

When making use of equations 5 and 6 for large but finite limits, we will use the term "infinite limits approximations." These equalities are in fact considered properties of Fresnel integrals, as is

$$C(0) \quad = \quad S(0) = 0. \tag{7}$$

These will prove useful in our proof below.

2.3 Other Properties

We also note that the odd symmetry of the Fresnel integrals allows other observations among which are:

$$\int_{-u}^{0} \cos\left(\frac{\pi}{2}x^2\right) \quad = \quad C(u) \tag{8}$$

$$\int_{-u}^{0} \sin\left(\frac{\pi}{2}x^2\right) \quad = \quad S(u) \tag{9}$$

$$\int_{-u}^{u} \cos\left(\frac{\pi}{2}x^2\right) \quad = \quad 2C(u) \tag{10}$$

$$\int_{-u}^{u} \sin\left(\frac{\pi}{2}x^2\right) \quad = \quad 2S(u) \tag{11}$$

$$\int_{-\infty}^{\infty} \cos\left(\frac{\pi}{2}x^2\right) \quad = \quad 1 \tag{12}$$

$$\int_{-\infty}^{\infty} \sin\left(\frac{\pi}{2}x^2\right) \quad = \quad 1. \tag{13}$$

3 Detailed Proof of Concave Down Parabolic Phase for a DC-Centered Increasing Frequency Chirp Signal

The proof below consists of several steps, each of which is covered in its own subsection. We begin by defining an increasing frequency DC-centered chirp signal and considering the real and imaginary parts of its FFT. Next, we approximate the sums therein with integrals. Then, we manipulate these integrals into Fresnel integral form (seen in the previous section). Once in this form, we can apply relevant Fresnel integral approximations. Finally, using these closed form approximations for the real and imaginary parts of the FFT, we obtain an elegant expression revealing concave down parabolic phase. Final subsections show how we may treat the cases of decreasing frequency chirps and signals whose center frequency is not DC.

3.1 Definition of a Linear Frequency Chirp Function and its FFT

We begin by considering the windowed discrete time function

$$y(n) \quad = \quad w(n)e^{i\alpha n^2} \tag{14}$$

where $w(n)$ is an $N-$sample (N odd) discrete time windowing function valued from $-(N-1)/2$ to $(N-1)/2$ and α is a positive constant equal to half the linear frequency increase per sample in radians. As noted earlier, we will consider the decreasing frequency chirp case in section 3.6.

3.1.1 Frequency Content Implied by α

The single parameter α was chosen for notational simplicity to represent the rate of linear frequency increase in the chirp signal. We now consider the frequencies actually represented. Since αn^2 represents the argument of our analytic signal, the frequencies contained correspond to $\frac{\Delta(\alpha n^2)}{\Delta n} = 2\alpha(n-0.5)$.[4]

Since we are in discrete time, the factor α needs to incorporate the sampling rate and the 2π factor required for representing discrete time frequency in radians per sample. Thus, to consider the actual signal frequency in Hz, we use $a = \frac{F}{2\pi}\alpha$ (or $\alpha = \frac{2\pi}{F}a$) where F is the sampling frequency and a is the actual signal frequency in Hz. Playing an analogous role to α, a is a positive constant equal to half the linear frequency increase in Hz per sample. To consider the actual frequencies of the signal, we thus have $2a(n-0.5)$.

We note that the mathematics require that the frequencies correspond to those not observed at actual time domain samples, but rather the frequencies at points in time between those samples (at $(n-0.5)$). This will not present a problem, as we will eventually use an integral approximation in our analysis whose midpoint rule requires us to use points half way between samples as bounds. This integral has an interval of $-N/2$ to $N/2$ and thus contains frequencies which are $2a(-N/2)$ to $2a(N/2)$ or, simplified, $-aN$ to aN. We may calculate the frequency bin numbers corresponding to these values as

$$\boxed{k_{\max} = \pm\frac{\alpha K N}{4\pi}} \tag{15}$$

where K is the length of the optionally zero padded FFT. If no zero padding is used, $K = N$ and we clearly have $k_{\max} = \pm\frac{\alpha N^2}{4\pi}$. We note that in any representation, y has a "center frequency" of zero (DC). In the time domain, this occurs at $n = 0$. (Cases of other center frequencies are also discussed below.)

We presently note that α must not be so large as to cause frequencies greater than the Nyquist frequency, namely $\frac{F}{2}$. Since the maximum frequencies occur at the edges of the time window, we have then, that $|aN| < \frac{F}{2}$. Thus $a < \frac{F}{2N}$ and, recalling our comment about α and a above, $\alpha < \frac{\pi}{N}$. These constraints will be important as we progress in the proof, and so we repeat them here:

$$\boxed{a < \frac{F}{2N}} \tag{16}$$

$$\boxed{\alpha < \frac{\pi}{N}} \tag{17}$$

As our proof progresses, we will see that a lower limit on α is also required for model validity. This is addressed in section 3.4.1.

[4] Choosing to use $\alpha/2$ in equation 14 would allow a more direct interpretation of the chirp parameter as the frequency increase in radians per sample. Our current choice, however, allows cleaner notation in the exponential arguments.

3.1.2 FFT of the Given Signal

We assume for now that $w(n)$ is a rectangular windowing function from $-\frac{N-1}{2}$ to $\frac{N-1}{2}$. (We will consider other windowing functions in a section below.) The DFT of our rectangular windowed $y(n)$ may be written

$$Y(k) = \sum_{n=-\frac{N-1}{2}}^{\frac{N-1}{2}} e^{i\alpha n^2} e^{-i2\pi kn/K} \tag{18}$$

$$= \sum_{n=-\frac{N-1}{2}}^{\frac{N-1}{2}} \exp(i(\alpha n^2 - 2\pi kn/K)). \tag{19}$$

where K is the length of the optionally zero padded transform. (If no zero padding is used, $K = N$.) Using Euler's identity ($e^{i\theta} = \cos(\theta) + i\sin(\theta)$), it is easy to see that the real and imaginary parts of $Y(k)$ are, respectively,

$$\Re Y(k) = \sum_{n=-(N-1)/2}^{(N-1)/2} \cos(\alpha n^2 - 2\pi kn/K) \tag{20}$$

$$\Im Y(k) = \sum_{n=-(N-1)/2}^{(N-1)/2} \sin(\alpha n^2 - 2\pi kn/K). \tag{21}$$

3.1.3 Intuitive Validity of Fresnel Analysis

The above expressions suggest – with their sums of sinusoids whose argument has an n^2 term – that a Fresnel analysis is appropriate. To illustrate this visually, we restate equations 20 and 21 as

$$\Re Y(k) = \sum_{n=-(N-1)/2}^{(N-1)/2} f_r(n,k) \tag{22}$$

$$\Im Y(k) = \sum_{n=-(N-1)/2}^{(N-1)/2} f_i(n,k). \tag{23}$$

where $f_r(n,k) = \cos(\alpha n^2 - 2\pi kn/K)$ and $f_i(n,k) = \sin(\alpha n^2 - 2\pi kn/K)$. We can now plot $f_r(n,k)$ and $f_i(n,k)$ for various values of k, along with the cumulative sums whose terminal values by definition reflect $\Re Y(k)$ and $\Im Y(k)$, respectively. Due to the similarity of $f_r(n,k)$ and $f_i(n,k)$, we presently plot only $f_r(n,k)$ for a simple example case in figure 3 below, in which $N = 201, K = N, a = 20$, and $F = 8000$. For the values of k in this figure, we see that the cumulative sum function appears visually similar to the Fresnel integrals (figure 1). We also see that its cumulative sum's terminal value appears to approach certain deterministic values. This is the intuition that motivates our Fresnel analysis.

To make note of the fact that the Fresnel analysis will not always be appropriate, we show a similar plot where the values of k render Fresnel analysis irrelevant. This is shown in figure 4, where we observe that the cumulative sums do not appear similar to Fresnel integrals in the way necessary to use Fresnel properties.

3.2 Approximation of the FFT Sums with Integrals

To apply the Fresnel analysis suggested above, we will need to convert the sums in equations 20 and 21 above to integrals, and will need to manipulate the resulting integrals into Fresnel integrals.

We begin this process by considering the above sums as midpoint approximations of an integral.[5] Stated formally, these approximations are:

$$\Re Y_a(k) = \int_{-N/2}^{N/2} \cos(\alpha n^2 - 2\pi kn/K)dn \approx \sum_{n=-(N-1)/2}^{(N-1)/2} \cos(\alpha n^2 - 2\pi kn/K) \tag{24}$$

$$\Im Y_a(k) = \int_{-N/2}^{N/2} \sin(\alpha n^2 - 2\pi kn/K)dn \approx \sum_{n=-(N-1)/2}^{(N-1)/2} \sin(\alpha n^2 - 2\pi kn/K). \tag{25}$$

where the subscript a reflects that the given expression is an inverse midpoint integral approximation. Note that we have omitted any reference to sampling frequency, since we are treating our integral as an approximation of the sum of the given samples, not as the area under the discrete curve.

[5] This reverses the paradigm often seen in introductory calculus, where the midpoint approximation is used to approximate integrals.

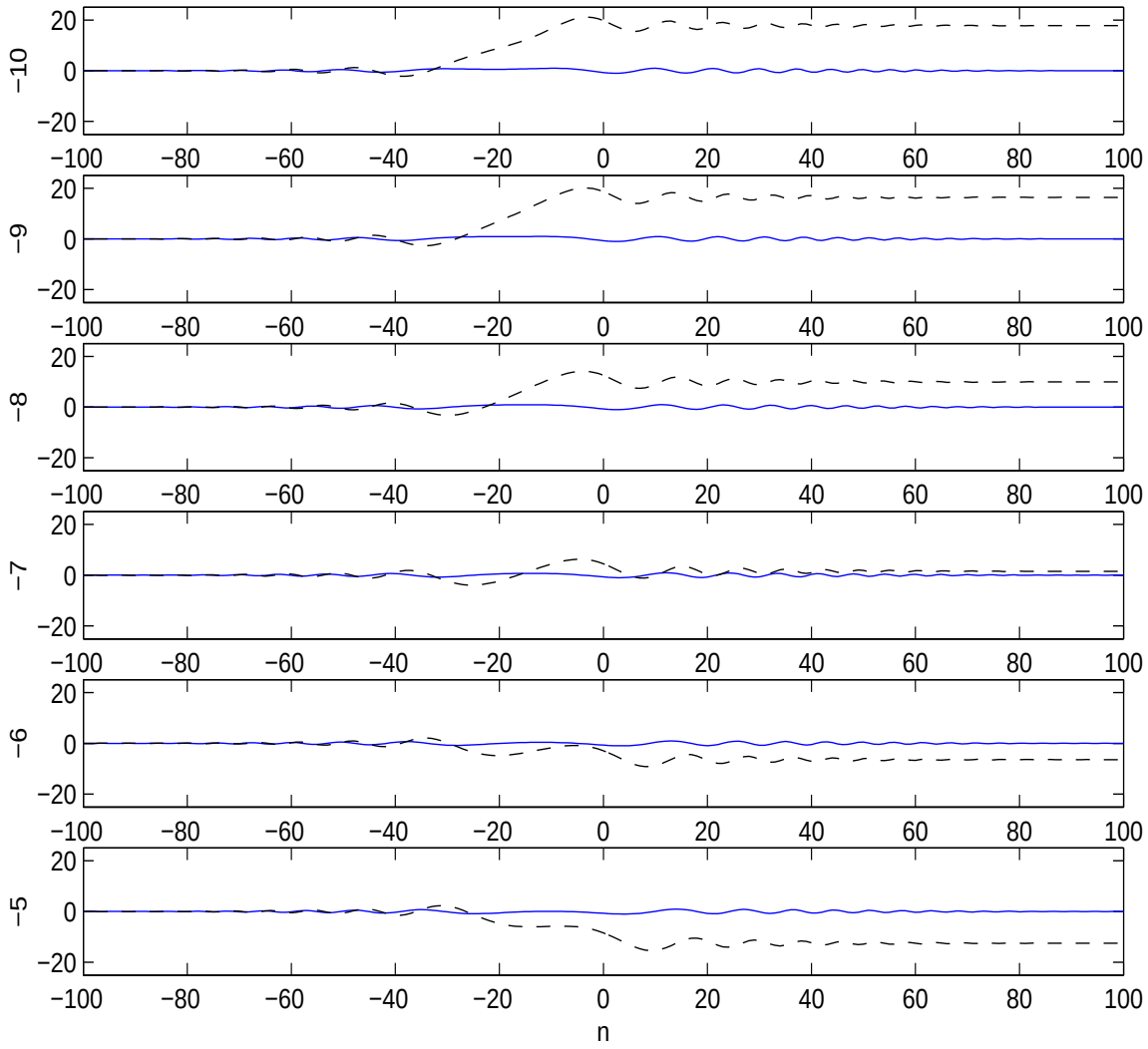

Figure 3: $f_r(n,k)$ (solid) and its cumulative sum (dashed) with terminal value $\Re Y(k)$ for various values of k (shown to the left of each plot). We notice that for these k values, the cumulative sum appears to be a modified Fresnel integral. This fact will motivate our Fresnel analysis in this section.

3.2.1 General Error Bound on the Inverse Midpoint Integral Approximation

The error introduced by the inverse approximation may be quantified by considering the sum as a truncated Taylor series expansion of the integral [1]. In the general case of the integral $\int_a^b f(x)dx$, this leads to an error bound of

$$|e_m| \leq \frac{M(b-a)^3}{24p^2} \tag{26}$$

where p is the number of subintervals between a and b and $|f''(x)| \leq M$. Applying this formula to the present case (over the variable n), we have

$$|e_m| \leq \frac{M(N/2-(-N/2))^3}{24N^2} = \frac{MN}{24}. \tag{27}$$

We note that we only consider approximating over N as opposed to K, since there is nothing to be gained in approximating the padding zeros. We also choose $K = N$ to simplify the number of potential cases (which does not affect any other pertinent values). We now must calculate M by considering $f''(n) \leq M$:[6]

$$f(n) = \cos(\alpha n^2 - 2\pi kn/N) \tag{28}$$

$$f'(n) = -\sin(\alpha n^2 - 2\pi kn/N)(2\alpha n - 2\pi k/N) \tag{29}$$

$$f''(n) = -\cos(\alpha n^2 - 2\pi kn/N)(2\alpha n - 2\pi k/N)^2 - \sin(\alpha n^2 - 2\pi kn/N)(2\alpha). \tag{30}$$

[6] We consider only the real part integral approximation though it should be apparent that the imaginary integral yields the same result.

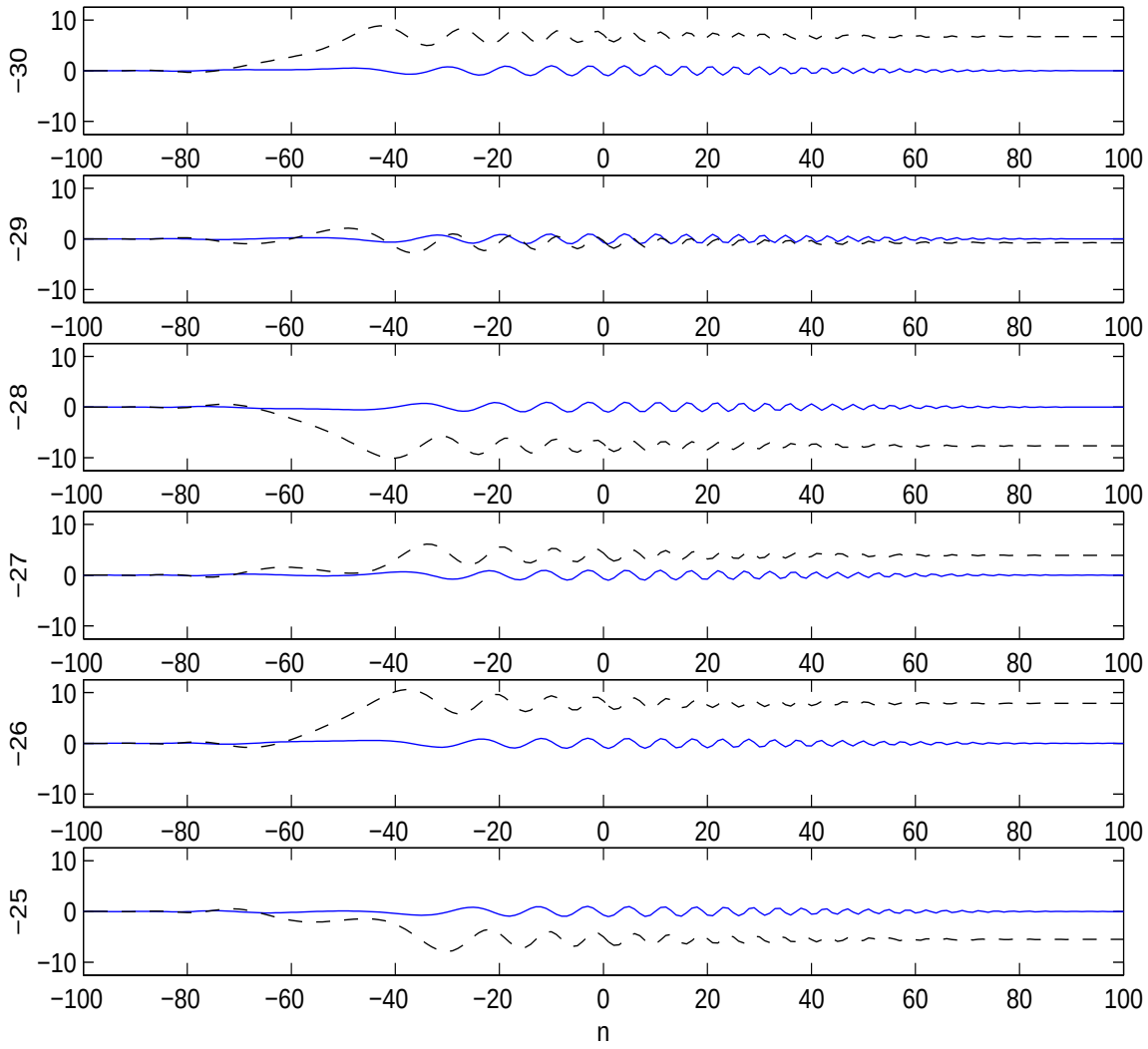

Figure 4: $f_r(n,k)$ (solid) and its cumulative sum (dashed) with terminal value $\Re Y(k)$ for various values of k (shown to the left of each plot). We notice that for these k values, the cumulative sum does not appear to be a modified Fresnel integral. This fact will motivate constraints on our Fresnel analysis in this section.

In the worst case, the sine and cosine factors will be of magnitude 1, giving

$$|f''(n)| \quad \leq \quad |(2\alpha n - 2\pi k/N)^2 + 2\alpha| = M. \tag{31}$$

(We note that in actuality, both functions can never be 1 at the same time, which leads to an overly conservative bound.) The worst case now occurs when n and k are large and opposite in sign. We model the error bound in this situation as:

$$|f''(n)| \quad \leq \quad (|2\alpha n| + |2\pi k/N|)^2 + 2\alpha = M. \tag{32}$$

Since n is our variable of integration, we maximize over it. (The variable k is best conceptualized as a constant that varies for each "case" of each different frequency bin in the FFT.) Since n can be no greater than $N/2$, we have that

$$|f''(n)| \quad \leq \quad (\alpha N + |2\pi k/N|)^2 + 2\alpha = M. \tag{33}$$

Substituting into equation 27, we now have that

$$|e_m(k)| \quad \leq \quad \frac{N}{24}\left((\alpha N + |2\pi k/N|)^2 + 2\alpha\right) \tag{34}$$

$$= \quad \frac{N}{24}\left(\alpha^2 N^2 + |4\pi k\alpha| + \frac{4\pi^2 k^2}{N^2} + 2\alpha\right) \tag{35}$$

$$= \quad \frac{1}{24}\left(2\alpha N + \frac{4\pi^2 k^2 \alpha}{N} + \alpha^2 N^3 + |4\pi k N\alpha|\right). \tag{36}$$

We observe that the error bound used here is overly conservative for two reasons. First, the assumption we made about the sinusoids being 1 was overly conservative as noted above. Second, the given bound implicitly assumes that the integrand varies as rapidly in general as it does in its most rapidly varying portions, namely the edges of the window where $n = \frac{N}{2}$. Thus, any term containing N in the numerator is overly conservative. We consider a tighter bound below.

3.2.2 Tighter Error Bound on the Inverse Midpoint Integral Approximation

Presently, we derive a tighter bound with our previous comments on equation 36 in mind. We divide up the integral into an arbitrary number of integer-width intervals, each with a lesser error bound than that given above (with the exception of those at the frame edges). The optimal case occurs when we simply choose N subintervals – one for each sample – so that the bound is different (and minimal) for each sample. This way, the high error in the most rapidly varying parts of the function will only be considered in the segments in which it may occur. Having segmented the signal this way, we then sum the error bounds for each sample to obtain the overall bound. Applying equation 27 each of N times gives

$$|\mathring{e}_m| \leq \sum_{n=-\frac{N-1}{2}}^{\frac{N-1}{2}} \frac{M_n 1^3}{24 \cdot 1^2} \tag{37}$$

where M_n is the bound M for the subinterval whose value is approximated by the sample n (obtained from each of N individual values of $|f''(n)|$). The number 1 is seen twice: in the numerator as the interval width and in the denominator as the number of subintervals. Continuing the above calculation by looking at M_n, we have:

$$M_n \geq \sum_n \left(\left(2\alpha n - \frac{2\pi k}{N} \right)^2 + 2\alpha \right) 1 \tag{38}$$

$$= 2\alpha N + \sum_n \left(4\alpha^2 n^2 - \frac{4\alpha n \pi k}{N} + \frac{4\pi^2 k^2}{N^2} \right) \tag{39}$$

$$= 2\alpha N + \frac{N 4\pi^2 k^2}{N^2} + 4 \sum_n \left(\alpha^2 n^2 - \frac{\alpha n \pi k}{N} \right). \tag{40}$$

We now observe that because of the symmetry of our sum, we may drop out the second term in the sum since it is an odd function. We also see that the remaining sum may itself be approximated using the inverse midpoint rule, generating $4(2\frac{\alpha^2}{3}(\frac{N}{2})^3) + e_m$ where $e_m \leq 2\alpha^2 N/24$. Continuing, we thus have

$$M_n \geq 2\alpha N + \frac{4\pi^2 k^2}{N} + 4\left(2\frac{\alpha^2}{3} \left(\frac{N}{2} \right)^3 \right) + 2\alpha^2 N/24 \tag{41}$$

$$= 2\alpha N + \frac{4\pi^2 k^2}{N} + \frac{8\alpha^2 N^3}{24} + \frac{2\alpha^2 N}{24}. \tag{42}$$

Substituting back into equation 37, we thus have

$$\boxed{|\mathring{e}_m| = \frac{1}{24}\left(2\alpha N + \frac{4\pi^2 k^2}{N} + \frac{\alpha^2 N^3}{3} + \frac{\alpha^2 N}{12} \right).} \tag{43}$$

We now verify that this bound is tighter than or equal to that given in equation 36. We start by assuming this as fact, and show that the fact is necessarily true.

$$|\mathring{e}_m| \leq |e_m| \tag{44}$$

$$\frac{1}{24}\left(2\alpha N + \frac{4\pi^2 k^2}{N} + \frac{\alpha^2 N^3}{3} + \frac{\alpha^2 N}{12} \right) \leq \frac{1}{24}\left(2\alpha N + \frac{4\pi^2 k^2}{N} + N^3\alpha^2 + |4\pi k N \alpha| \right) \tag{45}$$

$$\frac{\alpha^2 N^3}{3} + \frac{\alpha^2 N}{12} \leq N^3\alpha^2 + |4\pi k N \alpha| \tag{46}$$

$$\frac{\alpha^2 N}{12} \leq \frac{2N^3\alpha^2}{3} + |4\pi k N \alpha| \tag{47}$$

$$\frac{\alpha^2}{4} \leq 2N^2\alpha^2 + |12\pi k \alpha| \tag{48}$$

$$0 \leq \alpha^2 \left(2N^2 - \frac{1}{4} + \left| \frac{12\pi k}{\alpha} \right| \right) \tag{49}$$

This is necessarily true because $N \geq 1$. We observe by inspecting any line above (but the last), that as $\alpha \to 0$, the two limits become the same.

Even the tighter error bound given in equation 43 may seem significant. But we recall that, due to the constraints on α, the product αN will never be greater than π (which only occurs in the diabolical Nyquist frequency case), and in the case of actual audio signals will never even approach this value, causing all αN terms to be less than 1. We also note that this implies that $\alpha < \frac{1}{N}$. In order to determine the relative size of our error completely, we need to know the size of our "good data" estimates. Looking ahead in the proof, we know that our good data will take the form of sinusoids modulated by a raised cosine of magnitude $\sqrt{\frac{2\pi}{\alpha}}$. Recalling our observation about α above, this modulation amplitude is always at least $\sqrt{2\pi N}$.

Armed with these observations, we consider each term in equation 43. The first and fourth terms will be less than $\frac{1}{12}$ and $\frac{1}{N \cdot 288}$, respectively, and are thus small relative to the good data. The third term will be bounded by $\frac{N}{72}$, which is in general small compared to $\sqrt{2\pi N}$. To be more specific, we only require that $\frac{N}{72} \ll \sqrt{\frac{2\pi}{\alpha}}$. This is guaranteed when $N \ll 10368\pi$, a condition that will prove easy to satisfy in general. Considering the second term (in the no zero padding case for simplicity) we know that the largest k value used will be $k_{\max} = \pm\frac{\alpha N^2}{4\pi}$. Substituting this into the second term and simplifying, we find that the second term is bounded by $\frac{1}{288}$, again small relative to the good data. As before, we note that these error bounds are worst case bounds that in reality will not often be seen.

We include a practical example in figure 5. Therein, we see the the real and imaginary parts of an example $Y(k)$ and the error bound given in equation 43, also function of k.

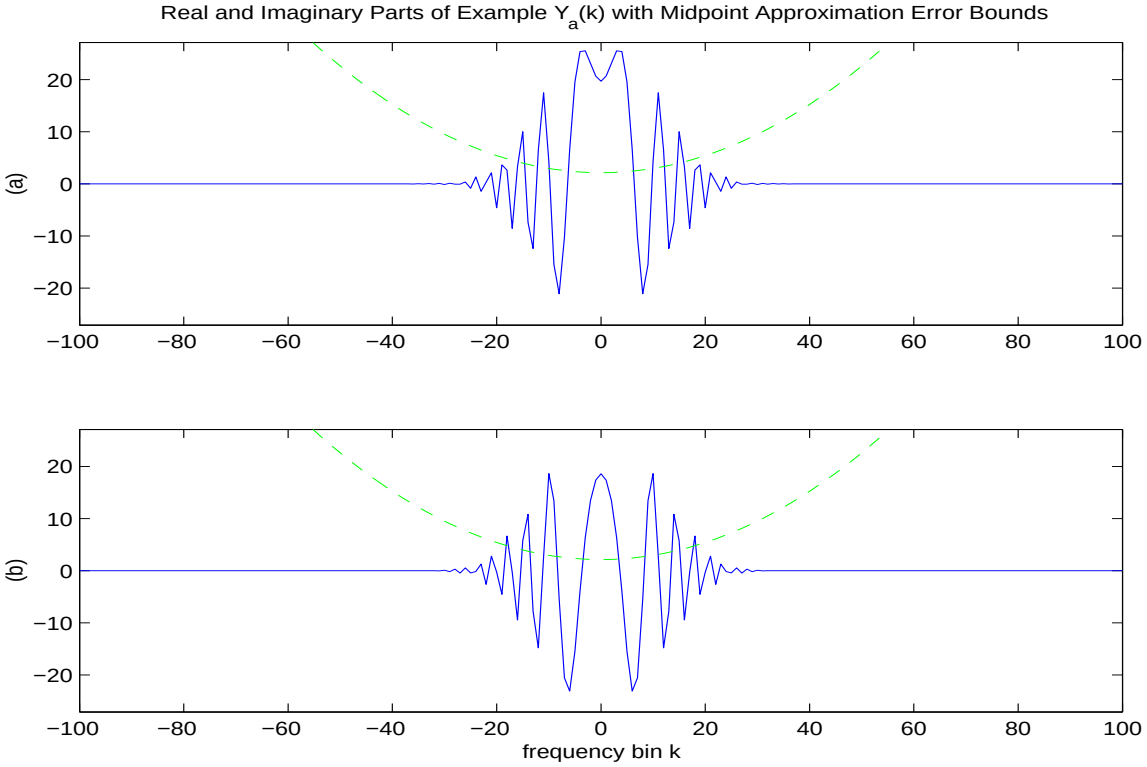

Figure 5: The real and imaginary parts of an example $Y(k)$ (solid) (with $\alpha = 0.004280$, $F = 8000$, $K = N = 201$, and a Hann windowing function) and the inverse midpoint approximation error (dashed).

3.3 Manipulation of the Integrals into Fresnel Integrals

Having satisfied ourselves that we may use integrals to approximate the FFT sums, we now apply algebraic manipulations to convert the integrals in equations 24 and 25 into Fresnel integrals.

First, we consider the argument of these sinusoids as a quadratic in n, for which we may complete the square to obtain:

$$\alpha n^2 - 2\pi k n/K = \alpha\left(n - \frac{\pi k}{K\alpha}\right)^2 - \frac{\pi^2 k^2}{K^2 \alpha}.$$

This gives

$$\Re Y_a(k) \quad = \quad \int_{-N/2}^{N/2} \cos\left(\alpha\left(n - \frac{\pi k}{K\alpha}\right)^2 - \frac{\pi^2 k^2}{K^2\alpha}\right) dn \tag{50}$$

$$\Im Y_a(k) = \int_{-N/2}^{N/2} \sin\left(\alpha\left(n-\frac{\pi k}{K\alpha}\right)^2 - \frac{\pi^2 k^2}{K^2\alpha}\right) dn. \tag{51}$$

Now, applying the trigonometric identities

$$\cos(A-B) = \cos(A)\cos(B) + \sin(A)\sin(B)$$

$$\sin(A-B) = \sin(A)\cos(B) - \cos(A)\sin(B)$$

yields

$$\Re Y_a(k) = \cos\left(\frac{\pi^2 k^2}{K^2\alpha}\right)\int_{-N/2}^{N/2}\cos\left(\alpha\left(n-\frac{\pi k}{K\alpha}\right)^2\right)dn + \sin\left(\frac{\pi^2 k^2}{K^2\alpha}\right)\int_{-N/2}^{N/2}\sin\left(\alpha\left(n-\frac{\pi k}{K\alpha}\right)^2\right)dn \tag{52}$$

$$\Im Y_a(k) = \cos\left(\frac{\pi^2 k^2}{K^2\alpha}\right)\int_{-N/2}^{N/2}\sin\left(\alpha\left(n-\frac{\pi k}{K\alpha}\right)^2\right)dn - \sin\left(\frac{\pi^2 k^2}{K^2\alpha}\right)\int_{-N/2}^{N/2}\cos\left(\alpha\left(n-\frac{\pi k}{K\alpha}\right)^2\right)dn. \tag{53}$$

Next, we make the change of variables

$$\begin{aligned} m &= n - \frac{\pi k}{K\alpha} \\ dn &= dm \end{aligned}$$

$$\begin{aligned} n &= -N/2 \Rightarrow m = -N/2 - \frac{\pi k}{K\alpha} \\ n &= N/2 \Rightarrow m = N/2 - \frac{\pi k}{K\alpha} \end{aligned}$$

giving

$$\Re Y_a(k) = \cos\left(\frac{\pi^2 k^2}{K^2\alpha}\right)\int_{-N/2-\frac{\pi k}{K\alpha}}^{N/2-\frac{\pi k}{K\alpha}}\cos\left(\alpha m^2\right)dm + \sin\left(\frac{\pi^2 k^2}{K^2\alpha}\right)\int_{-N/2-\frac{\pi k}{K\alpha}}^{N/2-\frac{\pi k}{K\alpha}}\sin\left(\alpha m^2\right)dm \tag{54}$$

$$\Im Y_a(k) = \cos\left(\frac{\pi^2 k^2}{K^2\alpha}\right)\int_{-N/2-\frac{\pi k}{K\alpha}}^{N/2-\frac{\pi k}{K\alpha}}\sin\left(\alpha m^2\right)dm - \sin\left(\frac{\pi^2 k^2}{K^2\alpha}\right)\int_{-N/2-\frac{\pi k}{K\alpha}}^{N/2-\frac{\pi k}{K\alpha}}\cos\left(\alpha m^2\right)dm. \tag{55}$$

Our final step is the substitution

$$\begin{aligned} \frac{\pi}{2}u^2 &= \alpha m^2 \\ u &= \pm\sqrt{\frac{2\alpha}{\pi}}m \\ dm &= \pm\sqrt{\frac{\pi}{2\alpha}}du \end{aligned}$$

$$\begin{aligned} m &= -N/2 - \frac{\pi k}{K\alpha} \Rightarrow u = \pm\sqrt{\frac{2\alpha}{\pi}}\left(-\frac{N}{2} - \frac{\pi k}{\alpha K}\right) \\ m &= N/2 - \frac{\pi k}{K\alpha} \Rightarrow u = \pm\sqrt{\frac{2\alpha}{\pi}}\left(\frac{N}{2} - \frac{\pi k}{\alpha K}\right), \end{aligned}$$

which yields

$$\boxed{\Re Y_a(k) = \pm\sqrt{\frac{\pi}{2\alpha}}\left(\cos\left(\frac{\pi^2 k^2}{K^2\alpha}\right)\int_{\pm\sqrt{\frac{2\alpha}{\pi}}\left(\frac{N}{2}-\frac{\pi k}{\alpha K}\right)}^{\pm\sqrt{\frac{2\alpha}{\pi}}\left(\frac{N}{2}-\frac{\pi k}{\alpha K}\right)}\cos\left(\frac{\pi}{2}u^2\right)du + \sin\left(\frac{\pi^2 k^2}{K^2\alpha}\right)\int_{\pm\sqrt{\frac{2\alpha}{\pi}}\left(-\frac{N}{2}-\frac{\pi k}{\alpha K}\right)}^{\pm\sqrt{\frac{2\alpha}{\pi}}\left(\frac{N}{2}-\frac{\pi k}{\alpha K}\right)}\sin\left(\frac{\pi}{2}u^2\right)du\right)} \tag{56}$$

$$\boxed{\Im Y_a(k) = \pm\sqrt{\frac{\pi}{2\alpha}}\left(\cos\left(\frac{\pi^2 k^2}{K^2\alpha}\right)\int_{\pm\sqrt{\frac{2\alpha}{\pi}}\left(-\frac{N}{2}-\frac{\pi k}{\alpha K}\right)}^{\pm\sqrt{\frac{2\alpha}{\pi}}\left(\frac{N}{2}-\frac{\pi k}{\alpha K}\right)}\sin\left(\frac{\pi}{2}u^2\right)du - \sin\left(\frac{\pi^2 k^2}{K^2\alpha}\right)\int_{\pm\sqrt{\frac{2\alpha}{\pi}}\left(-\frac{N}{2}-\frac{\pi k}{\alpha K}\right)}^{\pm\sqrt{\frac{2\alpha}{\pi}}\left(\frac{N}{2}-\frac{\pi k}{\alpha K}\right)}\cos\left(\frac{\pi}{2}u^2\right)du\right).} \tag{57}$$

We observe that we have obtained closed form expressions in terms of Fresnel integrals.

3.4 Application of Fresnel Integral Approximations

Given these Fresnel integrals just obtained, we may apply the approximations given in the Fresnel integral review in section 2, provided that the conditions specified therein are met. We will first discuss the large limits approximation while assuming a rectangle window. We then explore the effect of the Hann window on the validity of the large limits approximation, and make the discovery that the Hann window in effect converts the large limits approximation into the infinite limits approximation via liftering.

3.4.1 Rectangle Window: Large Fresnel Integral Limits Approximation

We recall from section 2 that we may apply the approximations in equations 3 and 4 provided that the limits of integration are much greater or lesser than 1 or -1 respectively. To make the problem more tractable, we presently restate the condition on the limits as: the limits of integration are greater than or lesser than $1 \cdot c$ or $-1 \cdot c$ respectively, where c is a constant we deem sufficiently large. Now, given a specified frame length N and chirp signal characterized by α, we may conceptualize these limits as functions of k. To verify that these limits satisfy the requirement, we must solve the inequalities

$$\sqrt{\frac{2\alpha}{\pi}}\left(-\frac{N}{2}-\frac{\pi k}{\alpha K}\right) < -1 \cdot c \qquad \text{and} \qquad \sqrt{\frac{2\alpha}{\pi}}\left(\frac{N}{2}-\frac{\pi k}{\alpha K}\right) > 1 \cdot c \tag{58}$$

for k to obtain

$$k < \frac{NK\alpha}{2\pi} - c\sqrt{\frac{K^2\alpha}{2\pi}} \qquad \text{and} \qquad k > -\frac{NK\alpha}{2\pi} + c\sqrt{\frac{K^2\alpha}{2\pi}} \tag{59}$$

or simply

$$|k| < \frac{NK\alpha}{2\pi} - c\sqrt{\frac{K^2\alpha}{2\pi}}. \tag{60}$$

Concerning our choice of c, we note that choosing the "risky" $c = 1$ yields fractional error bounds (deduced from figure 2) of about 14%. Choosing $c = 2$ drops this bound to 2.3%, and $c = 2.5$ leads to 1.3%. A decaying exponential may be roughly fit to the fractional error characteristic for purposes of choosing c based on the fractional error tolerated.[7]

Now, given a desired accuracy, we may view the large limits requirement either as a function of k or as a function of α. If the former, we may consider that the model is only valid for certain bins. This is not a complete picture, however, since we see below that in some cases, *no* choice of k will satisfy equation 60. Thus we must also consider the large limits requirement as a constraint on α values for which we may consider the model valid. The relationship of each of k and α to the large limits requirement is now discussed separately.

Satisfying Requirements for the Large Limits Approximation by Choice of k

Despite small errors when $c \geq 2$, equation 60 may raise the concern that k has been restricted significantly. To see if this is true, we compare the above bound to the positive and negative frequency bins representing the maximum frequency present in the signal, $\pm k_{\max} = \frac{NK\alpha}{4\pi}$ (equation 15). To do this rigorously, we define b as a constant between 0 and 1 indicating what fraction of $k_{\max}$ contains a valid range for our approximation. We can then solve for b to determine if we have significantly restricted the range of bins in which our approximation is valid. Expressing the constrained k in equation 60 as $b \cdot |k_{\max}|$, our constraint becomes:

$$b \cdot |k_{\max}| < \frac{KN\alpha}{2\pi} - c\sqrt{\frac{K^2\alpha}{2\pi}}. \tag{61}$$

Substituting from equation 15, this is

$$b\frac{\alpha KN}{4\pi} < \frac{\alpha KN}{2\pi} - c\sqrt{\frac{K^2\alpha}{2\pi}}. \tag{62}$$

Solving for b, we obtain

$$b < 2 - \frac{2c}{N}\sqrt{\frac{2\pi}{\alpha}}, \tag{63}$$

and solving for c, we obtain

$$c < (2-b)\frac{N}{2}\sqrt{\frac{\alpha}{2\pi}}. \tag{64}$$

We take a moment to consider consequences of this result. First, We see a tradeoff between accuracy of the approximation (achieved by requiring a large c value) and the size of the frequency range in which our approximation is valid (represented by b). Simply put, the higher quality approximation we wish to make, the smaller the range in which we may consider the approximation valid. The range of validity will become crucially important when we backsolve for α.

Second, we note that certain values of c and α can lead to b values outside the range (0,1]. A reasonably high α and low c in equation 63 may actually cause $b > 1$, suggesting that the approximation is valid *outside* the range

[7] We note that in practice, this is not necessary, as we will find that specifying other parameters is a more useful approach.

representing frequencies present in the signal. This case will not give rise to any special analysis, as we do not find that consideration of bins outside $k_{\max}$ enhances our analysis. Furthermore, doing so strains our inverse midpoint integral approximation above.

A more significant problem is that for a very small α, we get b values less than or equal to zero, implying that no frequency bins are valid for the approximation. Specifically, solving for α we have that

$$\alpha \quad > \quad 2\pi \left(\frac{N}{2c}(2-b)\right)^{-2}. \tag{65}$$

Though it may not be obvious from inspecting this equation, this is a nontrivial constraint on α for speech and music signals, even when $c \leq 1$. In such practical cases, the large limits approximation is often invalid by this metric, and an alternative model must be used.

To make this more concrete, we offer the example of a musical tone of frequency 440 Hz, sounded with a 14 Hz frequency vibrato at 6 pulses per second. Listening to such a signal reveals that this range and speed represent the largest musically realistic ("Wagnerian opera-singer") values for such parameters; anything larger or faster sounds machine-like. A frequency range half this size is in fact more typical (and to some, will sound more tasteful). Thus, the α representing the underlying quasi-linear piecewise frequency functions in our Wagnerian singer signal is a representative maximum. Given these parameters, we calculate the maximum α value by considering an FFT analysis frame that happens to catch the ideal point in time where, in one half vibrato pulse, the frequency range will change 14 Hz (from 433 Hz to 447 Hz) over a time period of 83.3 ms. Assuming a sampling rate $F = 10000$ Hz for convenience, we thus have a 14 Hz frequency change over 833 samples, or .0168 Hz per sample, yielding $a = .00840$. This in turn leads to $\alpha = \frac{2\pi}{10000}a = 5.28 \cdot 10^{-5}$. Comparing this to the minimum value required by equation 65 requires that we choose b and c values, which we modestly require to be 0.75 and 1.5, respectively. Doing so leads to $\alpha > 2\pi \left(\frac{833}{2 \cdot 1.5}(2-0.75)\right)^{-2} = 5.22 \cdot 10^{-5}$. We thus see the razor-thin margin for validity of this model; requiring greater accuracy in c or the more "tasteful" vibrato alluded to above would invalidate the model. Hence, the need for modified models summarized in appendix A and to be rigorously discussed in future writing.

Effect of α on Satisfying the Large Limits Approximation

We take a moment to further explore the relationship between α, k and the large limits approximation. As can be seen from inspecting equations 65 and 58, there is a nonlinear relationship between the limits and α, and therefore between the validity of the large limits approximation and α. In figure 6, we plot the limits as a function of k for each of 9 α values. In each plot, we use a horizontal range of $k \leq k_{\max}$, which necessarily is different for each plot since $k_{\max}$ is a function of α. We recall that the lower and upper limits must be outside -1 and 1 respectively in order to use the large limits approximation, and see that these point have been marked by horizontal dotted lines. The key observation here is that as α becomes small, the range over which the approximation holds decreases, until no range remains. Hence, our abovementioned claim that this approximation is not valid for very small α. We do, however, observe that the limits in those cases fall in a range where *other* approximations may be used. This is the modification alluded to just above, and will be covered in future writing. Such modifications are also summarized in appendix A.

Application of the Large Limits Approximation

Having restricted k and α as above, our approximations may be applied to $\Re Y_a(K)$ and $\Im Y_a(K)$. Defining $l_1 = \sqrt{\frac{2\alpha}{\pi}}\left(-\frac{N}{2} - \frac{\pi k}{\alpha K}\right)$ and $l_2 = \sqrt{\frac{2\alpha}{\pi}}\left(\frac{N}{2} - \frac{\pi k}{\alpha K}\right)$ for notational simplicity, we may now write

$$\int_{\pm l_1}^{\pm l_2} \cos\left(\frac{\pi}{2}u^2\right) du \quad \approx \quad \pm\left(1 + \frac{1}{-l_1\pi}\sin\left(\frac{\pi}{2}(-l_1)^2\right) + \frac{1}{l_2\pi}\sin\left(\frac{\pi}{2}(l_2)^2\right)\right) \tag{66}$$

$$\int_{\pm l_1}^{\pm l_2} \sin\left(\frac{\pi}{2}u^2\right) du \quad \approx \quad \pm\left(1 - \frac{1}{-l_1\pi}\cos\left(\frac{\pi}{2}(-l_1)^2\right) - \frac{1}{l_2\pi}\cos\left(\frac{\pi}{2}(l_2)^2\right)\right), \tag{67}$$

which we substitute into equations 56 and 57 to obtain

$$\begin{aligned} \Re Y_a(k) \quad \approx \quad & \sqrt{\frac{\pi}{2\alpha}}\left(\cos\left(\frac{\pi^2 k^2}{K^2\alpha}\right)\left(1 + \frac{1}{-l_1\pi}\sin\left(\frac{\pi}{2}(-l_1)^2\right) + \frac{1}{l_2\pi}\sin\left(\frac{\pi}{2}(l_2)^2\right)\right)\right. \\ & \left. + \sin\left(\frac{\pi^2 k^2}{K^2\alpha}\right)\left(1 - \frac{1}{-l_1\pi}\cos\left(\frac{\pi}{2}(-l_1)^2\right) - \frac{1}{l_2\pi}\cos\left(\frac{\pi}{2}(l_2)^2\right)\right)\right) \end{aligned} \tag{68}$$

$$\begin{aligned} x\Im Y_a(k) \quad \approx \quad & \sqrt{\frac{\pi}{2\alpha}}\left(\cos\left(\frac{\pi^2 k^2}{K^2\alpha}\right)\left(1 - \frac{1}{-l_1\pi}\cos\left(\frac{\pi}{2}(-l_1)^2\right) - \frac{1}{l_2\pi}\cos\left(\frac{\pi}{2}(l_2)^2\right)\right)\right. \\ & \left. - \sin\left(\frac{\pi^2 k^2}{K^2\alpha}\right)\left(1 + \frac{1}{-l_1\pi}\sin\left(\frac{\pi}{2}(-l_1)^2\right) + \frac{1}{l_2\pi}\sin\left(\frac{\pi}{2}(l_2)^2\right)\right)\right). \end{aligned} \tag{69}$$

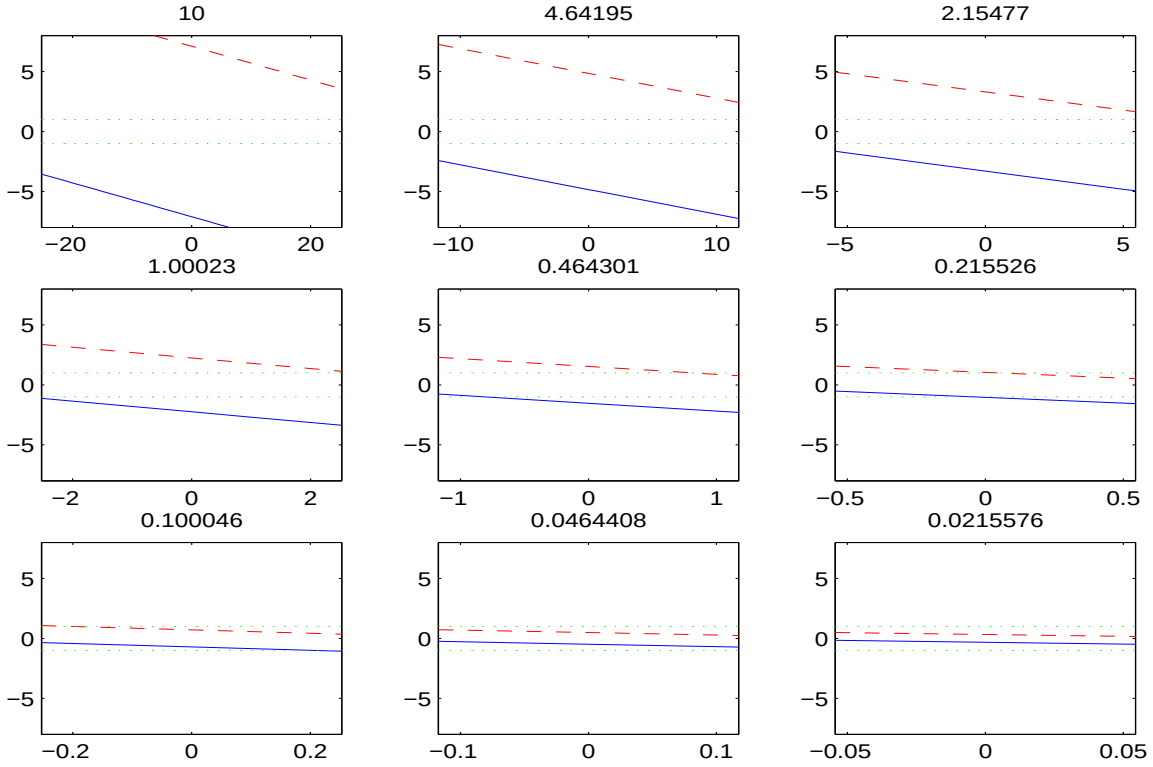

Figure 6: The lower (solid) and upper (dashed) limits as given in equation 58 as a function of k for 9 values of α (show above each plot). We see that as α becomes small, a smaller range – and eventually no range – of k is valid. In this example, $F = 8000$ and $K = N = 201$ for all α values.

We now apply the trigonometric identities

$$\cos(A)\cos(B) = \frac{1}{2}(\cos(A+B)+\cos(A-B)) \quad (70)$$

$$\cos(A)\sin(B) = \frac{1}{2}(\sin(B+A)+\sin(B-A)) \quad (71)$$

$$\sin(A)\sin(B) = \frac{1}{2}(\cos(A-B)-\cos(A+B)) \quad (72)$$

and, letting $\phi = \frac{\pi^2 k^2}{K^2 \alpha}$ to make the notation cleaner, we get:

$$\begin{aligned}\Re Y_a(k) \approx & \sqrt{\frac{\pi}{2\alpha}}\left[\cos(\phi)+\frac{1}{2}\frac{1}{-l_1\pi}\left(\sin\left(\frac{\pi}{2}l_1^2+\phi\right)+\sin\left(\frac{\pi}{2}l_1^2-\phi\right)\right)+\frac{1}{2}\frac{1}{l_2\pi}\left(\sin\left(\frac{\pi}{2}l_2^2+\phi\right)+\sin\left(\frac{\pi}{2}l_2^2-\phi\right)\right)\right. \\ & \left.+\sin(\phi)-\frac{1}{2}\frac{1}{-l_1\pi}\left(\sin\left(\phi+\frac{\pi}{2}l_1^2\right)+\sin\left(\phi-\frac{\pi}{2}l_1^2\right)\right)-\frac{1}{2}\frac{1}{l_2\pi}\left(\sin\left(\phi+\frac{\pi}{2}l_2^2\right)+\sin\left(\phi-\frac{\pi}{2}l_2^2\right)\right)\right] \quad (73)\end{aligned}$$

$$\begin{aligned}\Im Y_a(k) \approx & \sqrt{\frac{\pi}{2\alpha}}\left[\cos(\phi)-\frac{1}{2}\frac{1}{-l_1\pi}\left(\cos\left(\phi+\frac{\pi}{2}l_1^2\right)+\cos\left(\phi-\frac{\pi}{2}l_1^2\right)\right)-\frac{1}{2}\frac{1}{l_2\pi}\left(\cos\left(\phi+\frac{\pi}{2}l_2^2\right)+\cos\left(\phi-\frac{\pi}{2}l_2^2\right)\right)\right. \\ & \left.-\sin(\phi)-\frac{1}{2}\frac{1}{-l_1\pi}\left(\cos\left(\phi-\frac{\pi}{2}l_1^2\right)-\cos\left(\phi+\frac{\pi}{2}l_1^2\right)\right)-\frac{1}{2}\frac{1}{l_2\pi}\left(\cos\left(\phi-\frac{\pi}{2}l_2^2\right)-\cos\left(\phi+\frac{\pi}{2}l_2^2\right)\right)\right]. \quad (74)\end{aligned}$$

Regrouping common terms, we see that

$$\Re Y_a(k) \approx \sqrt{\frac{\pi}{2\alpha}}\left[\cos(\phi)+\frac{1}{l_1\pi}\sin\left(\phi-\frac{\pi}{2}l_1^2\right)+\sin(\phi)-\frac{1}{l_2\pi}\sin\left(\phi-\frac{\pi}{2}l_2^2\right)\right] \quad (75)$$

$$\Im Y_a(k) \approx \sqrt{\frac{\pi}{2\alpha}}\left[\cos(\phi)+\frac{1}{l_1\pi}\cos\left(\phi-\frac{\pi}{2}l_1^2\right)-\sin(\phi)-\frac{1}{l_2\pi}\cos\left(\phi-\frac{\pi}{2}l_2^2\right)\right]. \quad (76)$$

After so much discussion, this is not an entirely satisfying result; though the above equations are highly accurate, they are cumbersome and not readily manipulated into an elegant closed form expression for the phase of $Y_a(k)$. Fortunately, we realize that the approximations can be further simplified if we can eliminate the second and fourth sinusoidal terms in each. We will show that this can be done in either of two ways:

- Assume directly that the limits are well-approximated by infinity (rather than simply being much greater than 1). This is, in actuality, claiming that the "ringing" seen in Fresnel integrals has died out by the end of the particular integration frame. (Recall figure 3, which shows several such frames.) This allows us to simplify equations 66 and 67 to equal simply 1 (the infinite limits approximation), resulting in the dropping of the aforementioned sinusoidal terms. Making this claim without actually using a longer window, however,is a mathematical disaster. Doing so introduces so much Fresnel approximation error that the model becomes irrelevant. Hence, this approach is relegated to an appendix.
- Lifter out the offending sinusoids. As we will see, this can in fact be done by choosing a different time domain windowing function. The importance of this method is that it allows us to maintain the same error bounds as for the rectangle window with the large limits approximation, while yielding the desired invertible expression.

In the next subsection, we consider the second method. Therein we also show a very elegant fact: two ways of conceptualizing the attenuation of the sinusoids are mathematically equivalent. Those methods are the liftering mentioned in the second bullet above, and consideration of the Hann window as a direct attenuator of Fresnel ringing in the time domain.

3.4.2 Hann Window: Large and Infinite Limits Approximations

Motivation

In order to understand why a different windowing function can help simplify the approximations in equations 75 and 76, we must consider the root cause of the complicated expressions. This cause is the "ringing" inherent in Fresnel integrals. The large limits expressions approximate this ringing, with their sinusoidal terms. Hence, if we could attenuate the ringing to the point of an acceptable error, we could greatly simplify equations 75 and 76 by dropping the newly-irrelevant sinusoidal terms. Doing so is equivalent to treating the limits as quasi-infinite.

In fact, we can perform this attenuation by using a Hann window function. The effect of Hann windowing on ringing is illustrated in figure 7. Therein, we show the function representing the integrand (or sum argument) for the real part of $Y(k)$ for an arbitrarily chosen valid bin k_0, along with its cumulative sum.[8] To interpret this plot, we recall that $Y(k_0)$ is – by definition – equal to the last value of the cumulative sum (that seen at the rightmost edge of the window). We see that the ringing is attenuated in the cumulative sum – and the underlying function – in the Hann window plot, but not in the rectangle window plot.

Actually proving that the approximation given in equations 75 and 76 may be simplified as a result of the aforementioned ringing attenuation is another matter. To do this, we consider the effect of a Hann windowing function as a frequency domain *lifter*. We start by using the large limits approximation, and show that applying the Hann window allows us to modify the approximation into a more convenient and brief form. This form is very similar to that obtained by using the infinite limits approximation, showing identical phase.

Hann Window Definitions: Time, Frequency, and Liftering

We begin our frequency domain proof by considering the so-called window transform of the time domain Hann window. Since the Hann window may be expressed in the time domain as

$$w(n) \quad = \quad \frac{1}{2} + \frac{1}{2}\cos\left(\frac{2\pi n}{N}\right), \tag{77}$$

its FFT (the window transform) is

$$W(k) \quad = \quad \frac{1}{2}\delta(k) + \frac{1}{4}\delta\left(k - \frac{K}{N}\right) + \frac{1}{4}\delta\left(k + \frac{K}{N}\right). \tag{78}$$

Such a function clearly acts as a weighted averager when convolved with a sequence, and thus may be thought of as a lowpass filter in whatever domain it may appear. Since we will be applying this "filter" in the frequency domain, we may adopt the terminology of cepstral analysis, and say that high *quefrency* ripples will will be attenuated by our lowpass *lifter*. It is easy to be more specific about the quefrency response, because – due to duality – we already have the FFT of the lifter in the form of its time domain response: a raised cosine (equation 77). We simply must interpret the "time axis" from $-\frac{N}{2}$ to $\frac{N}{2}$ as the "quefrency axis" from $-\pi$ to π radians per frequency sample. We make an important note about the zero padding case (when $K \neq N$). We see by inspection of equation 78 that this causes the delta functions to be interspersed with zero-valued samples in what is effectively an upsampling (or stretch) operation. From Fourier theory we know that this introduces squeezed repetition in the quefrency domain, causing different quefrencies to be attenuated.

Figure 8 should clarify these relationships. We see a 201-point Hann window in the time domain, the zero padded frequency domain, the quefrency domain without zero padding, and the quefrency domain with a factor of two zero

[8] The imaginary part gives a similar visual cumulative sum result and is thus not shown.

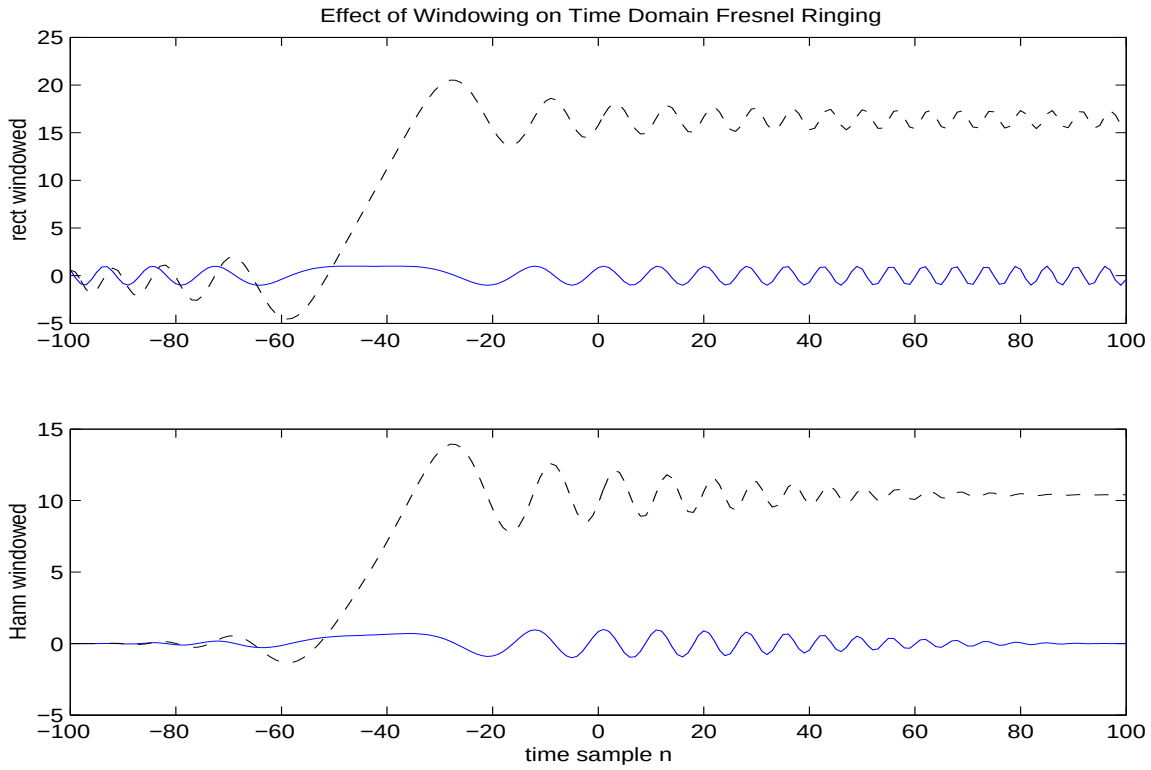

Figure 7: We plot the summed function of the form of equation 20 (solid line) along with its cumulative sum (dashed), for a frequency bin k satisfying our various constraints. We see that the rectangle window (top) does not attenuate the ringing of the underlying Fresnel integral while the Hann window (bottom) does. That is, we see the ringing die out in both the function and the cumulative sum in the Hann window case, but not in the rectangle window case.

padding. We see that in the no zero padding quefrency domain that quefrencies of π radians per sample will be completely attenuated and those of 0 radians per sample will be left untouched. In the zero padded quefrency domain, however, we see that quefrencies of odd integer multiples of $\frac{K}{N}\pi$ will be completely attenuated while those of even integer multiples of $\frac{K}{N}\pi$ will be left untouched. (This result agrees with the no zero padding case of $K = N$, as it must.)

Applying the Hann Window Lifter to the Sum-of-Sinusoids Expressions

We now consider what happens to our large limits approximation (equations 75 and 76) when we apply the lowpass lifter. This will be straightforward, as these approximations are in sum-of-sinusoids form. (Such expressions allow easy identification of the quefrencies in the signal.) We repeat the equations here for convenience:

$$\Re Y_a(k) \approx \sqrt{\frac{\pi}{2\alpha}}\left[\cos(\phi) + \frac{1}{l_1\pi}\sin\left(\phi - \frac{\pi}{2}l_1^2\right) + \sin(\phi) - \frac{1}{l_2\pi}\sin\left(\phi - \frac{\pi}{2}l_2^2\right)\right] \tag{79}$$

$$\Im Y_a(k) \approx \sqrt{\frac{\pi}{2\alpha}}\left[\cos(\phi) + \frac{1}{l_1\pi}\cos\left(\phi - \frac{\pi}{2}l_1^2\right) - \sin(\phi) - \frac{1}{l_2\pi}\cos\left(\phi - \frac{\pi}{2}l_2^2\right)\right]. \tag{80}$$

where $\phi = \frac{\pi^2 k^2}{K^2\alpha}$, $l_1 = \sqrt{\frac{2\alpha}{\pi}}\left(-\frac{N}{2} - \frac{\pi k}{\alpha K}\right)$, and $l_2 = \sqrt{\frac{2\alpha}{\pi}}\left(\frac{N}{2} - \frac{\pi k}{\alpha K}\right)$.

The quefrencies of the signals are seen by differentiating the arguments of the sinusoids. In the table below, we present each of the three unique arguments in the abbreviated notation used above, each such argument in the full notation, each argument simplified, and each argument's derivative with respect to k. We note that this last column thus shows the instantaneous quefrency as a function of k in radians per sample.

argument (abbrev.)	argument (full)	argument (simplified)	$\frac{d\arg}{dk}$
ϕ	$\frac{\pi^2 k^2}{K^2\alpha}$	$\frac{\pi^2 k^2}{K^2\alpha}$	$\frac{2\pi^2 k}{K^2\alpha}$
$\phi - \frac{\pi}{2}l_1^2$	$\frac{\pi^2 k^2}{K^2\alpha} - \frac{\pi}{2}\left(\frac{2\alpha}{\pi}\left(-\frac{N}{2} - \frac{\pi k}{\alpha K}\right)^2\right)$	$-\frac{\alpha N^2}{4} - \frac{N\pi k}{K}$	$-\frac{N\pi}{K}$
$\phi - \frac{\pi}{2}l_2^2$	$\frac{\pi^2 k^2}{K^2\alpha} - \frac{\pi}{2}\left(\frac{2\alpha}{\pi}\left(\frac{N}{2} - \frac{\pi k}{\alpha K}\right)^2\right)$	$-\frac{\alpha N^2}{4} + \frac{N\pi k}{K}$	$\frac{N\pi}{K}$

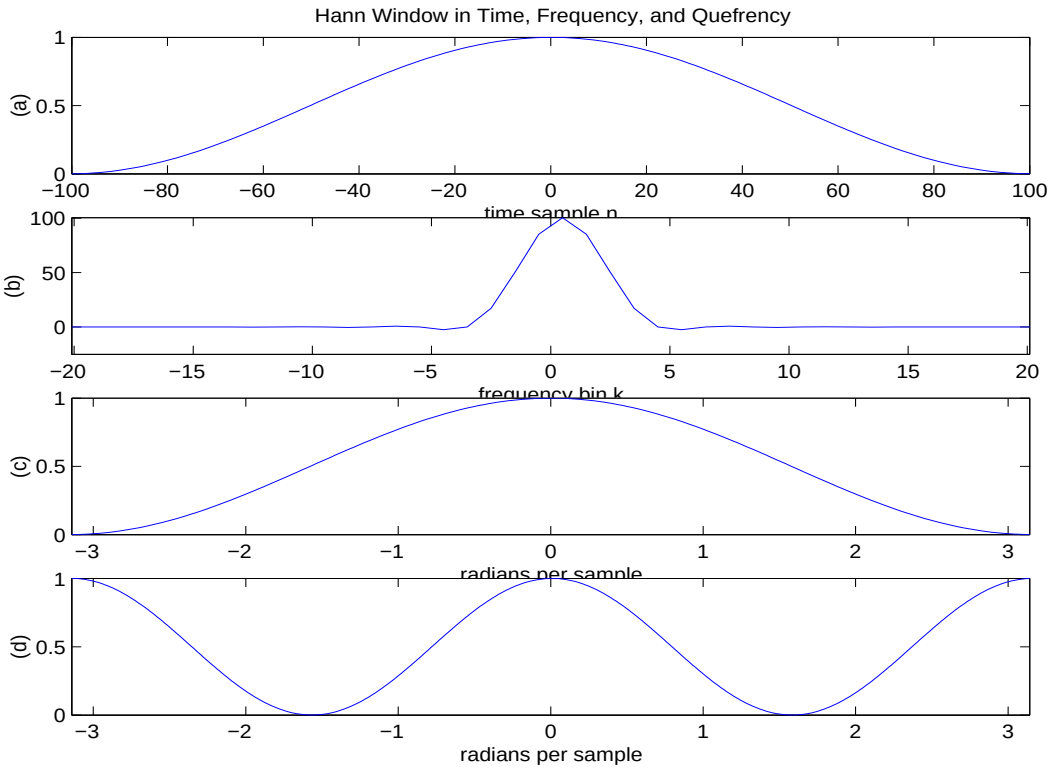

Figure 8: **(a)** 201-sample zero phase time domain Hann window; **(b)** zoom in of 2*201 point FFT of (a); **(c)** quefrency response of Hann window in (a) **(d)** quefrency response of zero padded ($K = 2 \cdot N$) Hann window.

We now consider the quefrency functions given in the rightmost column, relative to the quefrency attenuation we may expect due to the liftering Hann window. We see that the quefrencies for the second and third cases take on the values $\frac{-N\pi}{K}$ and $\frac{N\pi}{K}$, respectively, regardless of k. Looking at the quefrency response of our lifter, we see that these quefrencies are *completely* liftered out from our approximation. Thus, we may drop these terms from our approximations of $Y_a(k)$ (equations 75 and 76). We must also consider the effect of the lifter on the ϕ terms. Since the quefrency in those terms is given by $\frac{2\pi^2 k}{K^2\alpha}$, we know that they are attenuated by the filter according to its quefrency response, which attenuates quefrencies at odd integer multiples of $\frac{N\pi}{K}$. Thus, they are amplitude modulated by $\frac{1}{2} + \frac{1}{2}\cos\left(\frac{2\pi^2 k}{KN\alpha}\right)$. This leaves us with

$$\boxed{\Re Y_a(k) \approx \sqrt{\frac{\pi}{2\alpha}}\left(\frac{1}{2} + \frac{1}{2}\cos\left(\frac{2\pi^2 k}{KN\alpha}\right)\right)\left(\cos\left(\frac{\pi^2 k^2}{K^2\alpha}\right) + \sin\left(\frac{\pi^2 k^2}{K^2\alpha}\right)\right)} \tag{81}$$

$$\boxed{\Im Y_a(k) \approx \sqrt{\frac{\pi}{2\alpha}}\left(\frac{1}{2} + \frac{1}{2}\cos\left(\frac{2\pi^2 k}{KN\alpha}\right)\right)\left(\cos\left(\frac{\pi^2 k^2}{K^2\alpha}\right) - \sin\left(\frac{\pi^2 k^2}{K^2\alpha}\right)\right).} \tag{82}$$

We leave our expressions in this form to show the identical amplitude modulation of both the real and imaginary parts of $Y_a(k)$. Having achieved our final closed form expressions, we momentarily return to the infinite limits approximation. It is simple to verify that the infinite limits approximation has the same phase as that suggested by equations 81 and 82, since the infinite limits approximation allows us to state that

$$\int_{\pm\sqrt{\frac{2\alpha}{\pi}}\left(-\frac{N}{2}-\frac{\pi k}{\alpha K}\right)}^{\pm\sqrt{\frac{2\alpha}{\pi}}\left(\frac{N}{2}-\frac{\pi k}{\alpha K}\right)} \cos\left(\frac{\pi}{2}u^2\right)du \quad \approx \quad \pm\int_{-\infty}^{\infty}\cos\left(\frac{\pi}{2}u^2\right)du = \pm 1 \tag{83}$$

$$\int_{\pm\sqrt{\frac{2\alpha}{\pi}}\left(-\frac{N}{2}-\frac{\pi k}{\alpha K}\right)}^{\pm\sqrt{\frac{2\alpha}{\pi}}\left(\frac{N}{2}-\frac{\pi k}{\alpha K}\right)} \sin\left(\frac{\pi}{2}u^2\right)du \quad \approx \quad \pm\int_{-\infty}^{\infty}\sin\left(\frac{\pi}{2}u^2\right)du = \pm 1, \tag{84}$$

and the substitution of this into equations 56 and 57 allows us to conclude that

$$\Re Y_a(k) \quad \approx \quad \sqrt{\frac{\pi}{2\alpha}}\left(\cos\left(\frac{\pi^2 k^2}{K^2\alpha}\right) + \sin\left(\frac{\pi^2 k^2}{K^2\alpha}\right)\right) \tag{85}$$

$$\Im Y_a(k) \quad \approx \quad \sqrt{\frac{\pi}{2\alpha}} \left(\cos\left(\frac{\pi^2 k^2}{K^2 \alpha}\right) - \sin\left(\frac{\pi^2 k^2}{K^2 \alpha}\right) \right). \tag{86}$$

We see that equations 81 and 82 are identical to equations 85 and 86, but for the amplitude modulation due to the Hann lifter; *the phase given by both sets of equations will be identical.* Since this is true, we may call the result in equations 81 and 82 the amplitude modulated quasi-infinite limits approximation.

We make note that application of the Hann window does indeed make the "ringing" of the Fresnel integral negligible as we suspected. We see then, great benefit in using the Hann window, as it allows us to obtain such elegant and accurate expressions for $Y_a(k)$. We may now easily calculate the phase from equations 81 and 82 and note that we cannot do this from equations 75 and 76. This fact, coupled with the elegance of the phase result suggests that a practical invertible model requires the Hann window when the large limits approximation is applied as above. When applying different Fresnel approximation, however, the rectangle window case may still be useful. This is touched upon in appendix A and is to be covered in more detail in upcoming reports.

We also note that we did not incur any additional error in arriving at equations 81 and 82 for the Hann window, relative to that incurred when making the large limits approximation. We may view this fact in terms of model validity: the amplitude-modulated infinite limits approximation is valid for the Hann window and the large limits approximation is valid for the rectangle window, both within the same error bound. (Refer to equations 60 and 63). Neither approximation, however, is valid for the other window's case. (Refer to the discussion relating to equation 160.)

Figure 9 below shows an example application of the large limits approximation in the Hann window case. We see the real and imaginary parts of $Y(k)$ (solid), together with the estimates ($Y_a(k)$) obtained using equations 81 and 82 (dashed). Also plotted are the error bounds resulting from the large limits approximation (dot-dash). We do not show the bounds for the inverse midpoint integral approximation, because in practice, these worst-case bounds are never even approached, and lead to a mischaracterization of the error. The large limits approximation error, however, is a certainty.

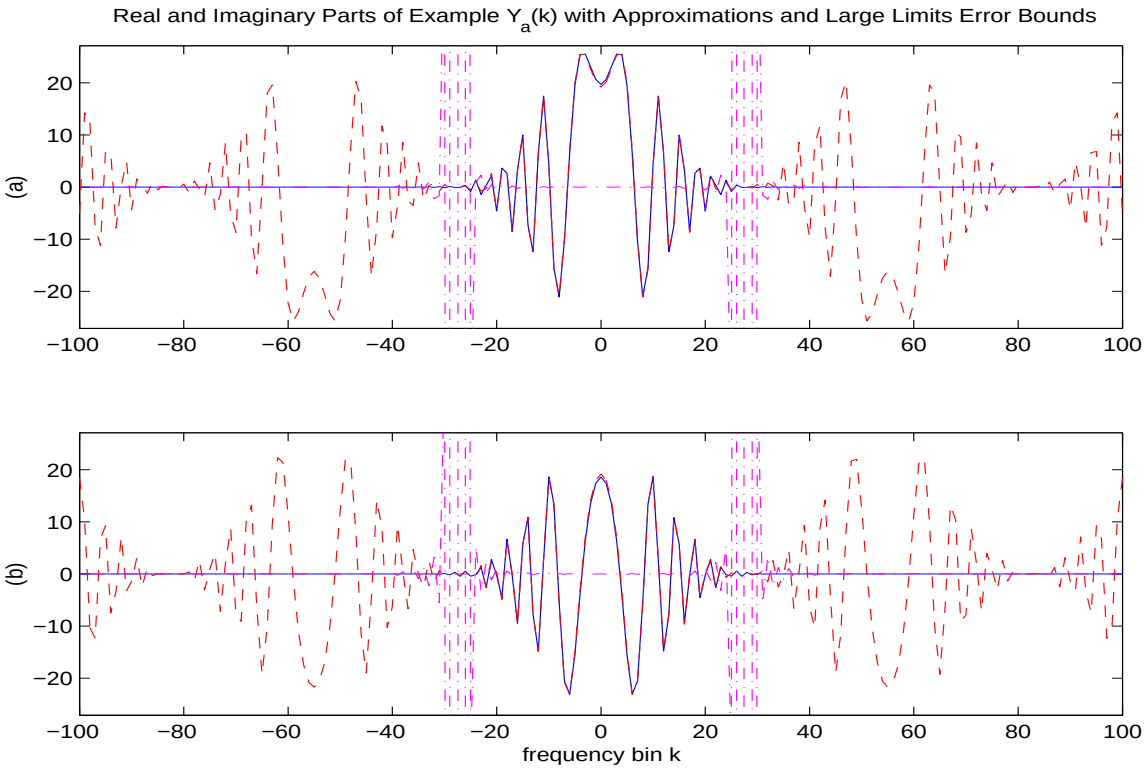

Figure 9: The real and imaginary parts of an example $Y(k)$ (solid) (with $\alpha = 0.004280$, $F = 8000$, $K = N = 201$, and a Hann windowing function) and the approximation obtained using equations 81 and 82 (dashed). Large limits approximation error bounds are also shown (dot-dash).

3.5 Hann Window / Infinite Limits Resulting Phase and Magnitude Approximation

3.5.1 Phase Approximation

Given the simpler approximations for the real and imaginary parts of $Y_a(k)$ in equations 81 and 82, we may obtain a closed form approximation for the phase as follows (here, we have again used $\phi = \frac{\pi^2 k^2}{K^2 \alpha}$ for notational simplicity):

$$\angle Y_a(k) \approx \angle\left(\sqrt{\frac{\pi}{2\alpha}}\left(\frac{1}{2}+\frac{1}{2}\cos\left(\frac{2\pi^2 k}{KN\alpha}\right)\right)(\cos(\phi)+\sin(\phi)+i(\cos(\phi)-\sin(\phi)))\right) \quad (87)$$

$$= \angle\left(\frac{e^{i\phi}+e^{-i\phi}}{2}+\frac{e^{i\phi}-e^{-i\phi}}{2i}+i\frac{e^{i\phi}+e^{-i\phi}}{2}-i\frac{e^{i\phi}-e^{-i\phi}}{2i}\right) \quad (88)$$

$$= \angle\left(\frac{e^{i\phi}+e^{-i\phi}-e^{i\phi}+e^{-i\phi}}{2}+\frac{e^{i\phi}-e^{-i\phi}-e^{i\phi}-e^{-i\phi}}{2i}\right) \quad (89)$$

$$= \angle\left(e^{-i\phi}-\frac{e^{-i\phi}}{i}\right) = \angle\left((1+i)e^{-i\phi}\right) = \angle\left(\sqrt{2}e^{i\pi/4}e^{-i\phi}\right) = \frac{\pi}{4}-\phi \quad (90)$$

$$= \frac{\pi}{4}-\frac{\pi^2 k^2}{K^2\alpha}. \quad (91)$$

This is clearly a downward pointing parabola as we sought. We repeat our conclusion and conditions for emphasis and clarity:

$$\boxed{\angle Y_a(k) \approx \frac{\pi}{4}-\frac{\pi^2 k^2}{K^2\alpha}} \qquad \begin{array}{l} \alpha > 0 \\ \alpha = \ \frac{1}{2}(\text{rate of linear frequency increase}) \\ |k| \le b \cdot k_{\max} \end{array} \quad (92)$$

Figure 10 illustrates the the phase of an example $Y(k)$ as well as the estimate obtained using equation 92. Due to the unwrap function used in the plot, we see that the phases do not line up exactly. Nonetheless, we see the great accuracy of the approximation by inspecting the first and second difference plots included below the phase plot. Error bounds for the large limits approximations are again shown (dot-dash). These were obtained by performing a standard error-propagation analysis [7]. A detailed derivation is given in appendix C. The observed irregularity of the error will ultimately lead to our preference of the magnitude approximation, described in the next subsection.

3.5.2 Magnitude Approximation

Inspection of equations 87 through 91 reveals that the magnitude of $Y_a(k)$ is approximated by

$$\boxed{|Y_a(k)| \approx \sqrt{\frac{\pi}{\alpha}}\left(\frac{1}{2}+\frac{1}{2}\cos\left(\frac{2\pi^2 k}{KN\alpha}\right)\right)} \quad (93)$$

under the same constraints on k as for the phase approximation.

Figure 11 illustrates the the magnitude of an example $Y(k)$ as well as the estimate obtained using equation 92. We see the great accuracy of the approximation. Again, the error bound for the large limits approximation is shown (dot-dash). We see that the error propagates in a more well-modeled way than for the phase approximation.

3.6 Modifications to Proof for Decreasing Frequency Chirp

Having achieved our proof's goal for the increasing frequency case just above, we now wish to apply a similar analysis to the case of a linearly *decreasing* frequency chirp. It is not possible to simply substitute $\alpha < 0$ in the above analysis, because doing so introduces imaginary numbers in the the $\sqrt{\frac{\pi}{2\alpha}}$ factors, preventing us from using the same real Fresnel properties used above. Thus we will slightly change our definitions and procedures.

We begin by redefining α so that it represents a decreasing frequency characteristic. Formally, we replace the initial reference to α in equation 14 with $-\alpha$ and require that α again be positive so that $-\alpha$ is always negative. Thus our new time domain signal is:

$$y_d(n) = w(n)e^{-i\alpha n^2}. \quad (94)$$

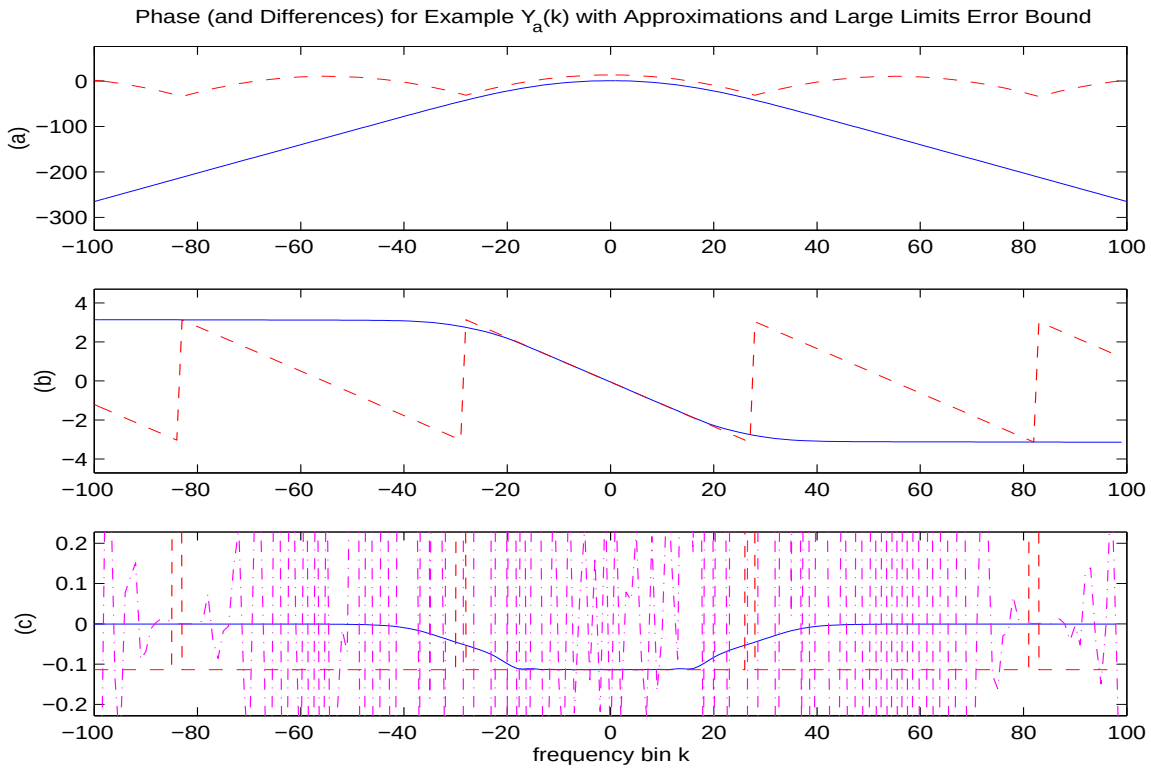

Figure 10: **(a)** The phase of an example $Y(k)$(solid) (with $\alpha = 0.004280$, $F = 8000$, $K = N = 201$, and a Hann windowing function) and the approximation obtained using equation 92 (dashed). **(b)** The first order difference of (a). **(c)** The second order difference of (a). Error bounds for the large limits approximation (dot-dash) are also shown.

where the subscript d denotes that this function represents a decreasing frequency chirp as opposed to the original increasing frequency chirp. Proceeding as above, equations 24 and 25 become

$$\Re Y_{da}(k) = \int_{-N/2}^{N/2} \cos(-\alpha n^2 - 2\pi kn/K)dn \approx \sum_{n=-(N-1)/2}^{(N-1)/2} \cos(-\alpha n^2 - 2\pi kn/K) \tag{95}$$

$$\Im Y_{da}(k) = \int_{-N/2}^{N/2} \sin(-\alpha n^2 - 2\pi kn/K)dn \approx \sum_{n=-(N-1)/2}^{(N-1)/2} \sin(-\alpha n^2 - 2\pi kn/K). \tag{96}$$

We presently consider $\Re Y_{da}(k)$ (equation 95). We observe that $\cos(-\alpha n^2 - 2\pi kn/N) = \cos(+\alpha n^2 + 2\pi kn/N)$ due to the evenness of the cosine function. Because the sum or integral we are considering is over a window or interval symmetric in the variable n, it is arbitrary whether we sum/integrate over $\cos(+\alpha n^2 + 2\pi kn/N)$ or $\cos(+\alpha n^2 - 2\pi kn/N)$. Thus,

$$\Re Y_{da}(k) = \int_{-N/2}^{N/2} \cos(-\alpha n^2 - 2\pi kn/K)dn \tag{97}$$

$$= \int_{-N/2}^{N/2} \cos(\alpha n^2 - 2\pi kn/K)dn \tag{98}$$

and the rest of the analysis for the real part is identical to that given above, so that for the Hann window case,

$$\Re Y_{da}(k) = \Re Y_a(k) \approx \sqrt{\frac{\pi}{2\alpha}} \left(\frac{1}{2} + \frac{1}{2}\cos\left(\frac{2\pi^2 k}{KN\alpha}\right)\right) \left(\cos\left(\frac{\pi^2 k^2}{K^2\alpha}\right) + \sin\left(\frac{\pi^2 k^2}{K^2\alpha}\right)\right). \tag{99}$$

We consider $\Im Y_{da}(k)$ (equation 96) in a similar fashion. Because sine is an odd function, $\sin(-\alpha n^2 - 2\pi kn/N) = -\sin(+\alpha n^2 + 2\pi kn/N)$. Again, since the sum or integral we are considering is over a window or interval symmetric in the variable n, it is arbitrary whether we sum/integrate over $\sin(+\alpha n^2 + 2\pi kn/N)$ or $\sin(+\alpha n^2 - 2\pi kn/N)$. Thus,

$$\Im Y_{da}(k) = \int_{-N/2}^{N/2} \sin(-\alpha n^2 - 2\pi kn/K)dn \tag{100}$$

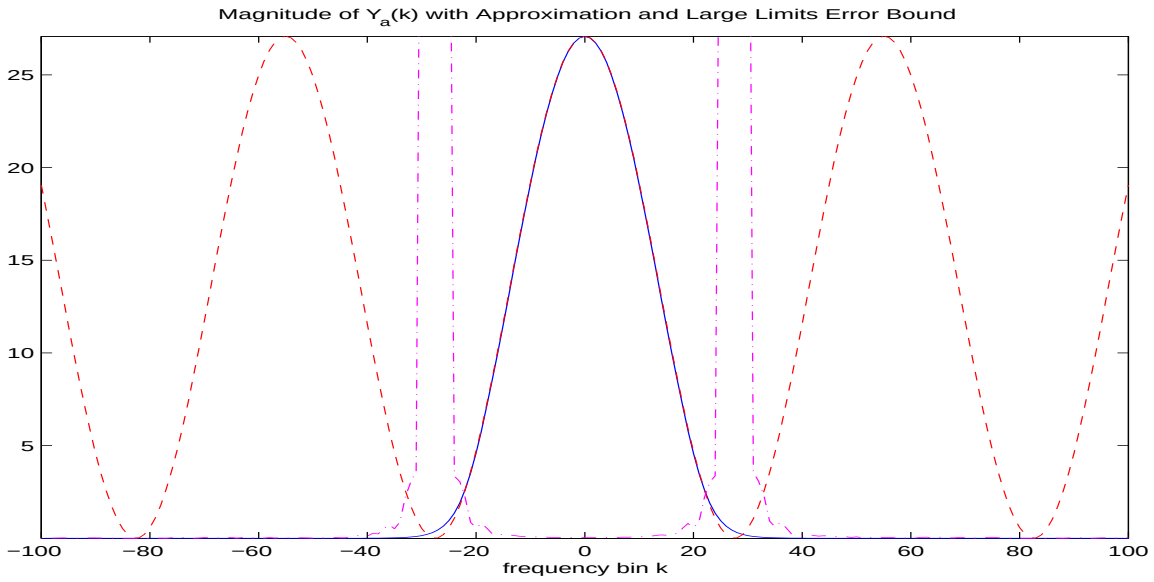

Figure 11: The magnitude of an example $Y(k)$(solid) (with $\alpha = 0.004280$, $F = 8000$, $K = N = 201$, and a Hann windowing function) and the approximation obtained using equation 93 (dashed). The error bound for the large limits approximation (dot-dash) is also shown.

$$= -\int_{-N/2}^{N/2} \sin(\alpha n^2 - 2\pi k n/K) dn \tag{101}$$

reflecting only a sign change from $\Im Y_a(k)$ in the original proof. This gives

$$\Im Y_{da}(k) = -\Im Y_a(k) \approx \sqrt{\frac{\pi}{2\alpha}} \left(\frac{1}{2} + \frac{1}{2}\cos\left(\frac{2\pi^2 k}{KN\alpha}\right)\right)\left(\sin\left(\frac{\pi^2 k^2}{K^2\alpha}\right) - \cos\left(\frac{\pi^2 k^2}{K^2\alpha}\right)\right). \tag{102}$$

We may now calculate the phase. To do so, we use the result in equation 91. Since we know that

$$\angle Y_a(k) = \arctan\left(\frac{\Im Y_a(k)}{\Re Y_a(k)}\right) = \frac{\pi}{4} - \frac{\pi^2 k^2}{K^2\alpha}, \tag{103}$$

we may conclude that

$$\angle Y_{da}(k) = \arctan\left(\frac{\Im Y_{da}(k)}{\Re Y_{da}(k)}\right) = \arctan\left(\frac{-\Im Y_a(k)}{\Re Y_a(k)}\right) = -\arctan\left(\frac{\Im Y_a(k)}{\Re Y_a(k)}\right) = -\frac{\pi}{4} + \frac{\pi^2 k^2}{K^2\alpha}. \tag{104}$$

This is an upward-pointing parabola, as we sought. We repeat our conclusion and conditions for this decreasing frequency case:

$$\boxed{\angle Y_{da}(k) \approx -\frac{\pi}{4} + \frac{\pi^2 k^2}{K^2\alpha}} \qquad \alpha = \frac{1}{2}(\text{rate of linear frequency decrease}) \qquad \begin{matrix}\alpha > 0 \\ |k| \le b \cdot k_{\max}\end{matrix} \tag{105}$$

We note that $|Y_{da}(k)|$ is identical to $|Y_a(k)|$ as given in equation 93:

$$\boxed{|Y_{da}(k)| = |Y_a(k)| \approx \sqrt{\frac{\pi}{\alpha}}\left(\frac{1}{2} + \frac{1}{2}\cos\left(\frac{2\pi^2 k}{KN\alpha}\right)\right)} \tag{106}$$

3.7 Generalizations of Proof to Nonzero Center Frequencies

As has been presented earlier by the author, it is possible to generalize this result to chirp signals centered about any frequency. This is of obvious importance when dealing with audio signals that are not centered about DC.

To see how this may be done, we must again consider our original expression for $Y(k)$ as first given in equation 19:

$$Y(k) = \sum_{n=-\frac{N-1}{2}}^{\frac{N-1}{2}} \exp(i(\alpha n^2 - 2\pi kn/K)). \tag{107}$$

When dealing with a signal of nonzero center frequency, this expression becomes

$$Y(k) = \sum_{n=-\frac{N-1}{2}}^{\frac{N-1}{2}} \exp(i(\alpha n^2 + \beta n - 2\pi kn/K)), \tag{108}$$

where β is the nonzero center frequency in radians per sample. It is equivalent to say:

$$Y(k) = \sum_{n=-\frac{N-1}{2}}^{\frac{N-1}{2}} \exp(i(\alpha n^2 - 2\pi \left(k - \frac{K\beta}{2\pi}\right) n/K)). \tag{109}$$

Thus, if we make the substitution $p = k - \frac{K\beta}{2\pi}$, we get

$$\boxed{Y\left(p + \frac{K\beta}{2\pi}\right) = \sum_{n=-\frac{N-1}{2}}^{\frac{N-1}{2}} \exp(i(\alpha n^2 - 2\pi pn/K))}. \tag{110}$$

We see that we may then continue our analysis as above, treating p as k and noting only that our entire $Y(k)$ expression is shifted by $\frac{K\beta}{2\pi}$. Thus, we obtain all the same approximations and conclusions already seen, but recognize that they apply to a different center frequency location. Recalling that sinusoids may be expressed as the superposition of two complex exponentials, we see that we now have a way of analyzing practical signals of nonzero center frequencies.

4 Model Inversion

Given our model, we may now consider its inversion. That is, given FFT magnitude and phase characteristics that could be generated by equations 92 and 93 (or 105 and 106), we claim that we have a linear frequency chirp signal. By the uniqueness of the non-aliased FFT, we claim that only a chirp signal characterized by a specific α could generate the same FFT characteristics.

Because both the phase and magnitude approximations for our model depend on α, we may attempt to invert either the phase equation or the magnitude equation to estimate α. To determine which will yield a more accurate estimate, we examine the way errors will affect either approximation. Up to this point, we have only considered errors as they effect the real and imaginary parts of the signal, not as they affect the phase and magnitude. Using standard error propagation analysis [7], it becomes evident that obtaining the magnitude (via squaring, addition, and square root operations) propagates error in a less data-degrading way than obtaining the second order phase difference (via division, arctangent, and two differencing operations). Empirical observation supports this claim: inverting the magnitude model as described below yields generally more accurate estimates of α than inverting the phase model. We provide details and results for both algorithms below.

4.1 Choosing the Relevant Frequency Range

Regardless of which model we invert (magnitude or phase), we must acknowledge that there are limitations on the frequency ranges in which either model is valid. These ranges are functions of the accuracy desired and of the true value of α. We already have noted in previous sections that as α becomes very small, the current model is not valid. Thus, none of the constraints on α for backsolving should cause alarm in this context. We present more detail below.

4.2 Inversion of the Magnitude Expression

4.2.1 Constraints

The magnitude expression inversion method will ultimately require that our model is valid throughout the frequency range representing frequencies in the signal. In terms of equation 63, we thus require that $b \geq 1$. Solving

$$b < 2 - \frac{2c}{N}\sqrt{\frac{2\pi}{\alpha}} \tag{111}$$

for α in this case shows that we require

$$\alpha \geq \frac{8\pi c^2}{N^2} \tag{112}$$

in order for our model to be valid. We may substitute this α value into equation 15 to see that we now require

$$k_{\max} \geq \frac{2c^2 K}{N}. \tag{113}$$

Inspecting equation 113, we may be tempted to think that choosing very small c will allow our model to be valid for an arbitrarily small range. But we recall that choosing $c < 1$ causes large error in the model, and that we can never specify $c < \frac{\sqrt{2}}{2}$, because doing so leads to a peak narrower than that prescribed by the Hann window transform for a quasistationary sinusoid. Specifically, if we set c this small, we have

$$k_{\max} = \frac{K}{N}, \tag{114}$$

which corresponds to the half height width of a Hann window transform. This is clearly not a valid model for α, because this narrow width should only be reached when $\alpha = 0$. We may actually view the peak width requirement as a constraint on α: it is only realistic to model α values that cause our model peak to be at least as wide as that of a Hann window main lobe. In fact, backsolving for α while requiring that the peak width be at least that of the main lobe width of a Hann window transform again yields $k_{\max} \geq \frac{2c^2 K}{N}$ as given in equation 113.

In summary, if choosing to model only α values that obey equation 112, we can guarantee accuracy specified by c by applying the magnitude inversion model only when $k_{\max} = \frac{2c^2 K}{N}$ results in a peak at least $\frac{K}{N}$ wide. As we will show in the next subsection, it is trivial to verify that the $k_{\max}$ requirement is satisfied.

4.2.2 Algorithm

We now consider inversion of the magnitude expression to estimate α. We begin by observing the half-height width k_{hh} of the smeared peak in the FFT magnitude domain.[9] Since the half height width will not necessarily occur at an integer k value, linear or other interpolation may be used to more accurately estimate k_{hh}. If our α value is large enough to guarantee that our approximation is valid at this point (discussed in the previous subsection), the half height width corresponds to $k_{\max}$ exactly. This is because the raised cosine is at half height when its argument is $\pm\frac{\pi}{2}$, and solving for k in this situation yields $|k| = \frac{\alpha K N}{4\pi}$, or $k_{\max}$.

As suggested previously, ensuring that our model is valid now becomes trivial: if $k_{hh} \geq \frac{2c^2 K}{N} > \frac{K}{N}$ for our desired c value, the model is valid.

We now calculate α by solving the half height expression for α. That is,

$$\boxed{|\alpha| \approx \frac{4\pi k_{hh}}{KN}}. \tag{115}$$

Having obtained this estimate of the magnitude of α, we need only determine its sign. This can be done by using the phase: if the phase is concave up, we know that α is negative, and that if the phase is concave down, α is positive. Since we only require knowledge of this simple fact, high accuracy in the phase is not required. To determine the concavity of the phase, we simply inspect the sign of the second order difference of the phase.

As noted above, the approximation in equation 115 will prove more reliable than the phase inversion model below due to error propagation. This is not to say that the phase inversion algorithm is devoid of merit; the error simply propagates in a less well-modeled way than in the magnitude case.

4.3 Inversion of the Phase Expression

Though inversion of the phase expression does not in general yield the same high quality results as inversion of the magnitude expression, we present constraints and an algorithm here for completeness.

4.3.1 Constraints

When inverting the phase characteristic, we need not rely on the half height criteria. As a result, we may choose $b < 1$ if we wish to obtain greater accuracy, rather than tolerate decreases in c to ensure that $b = 1$ as above.[10] To find the b value necessary to ensure the desired accuracy, we solve equation 63.

The only problem with finding b this way is that some estimate of α is required to choose b. This estimate may be obtained by using the half height model in the subsection above.

[9] In actuality, we could consider the three-quarter height or some other fraction. As witnessed in the discussion above, however, choosing half height greatly facilitates comparison with the window transform to check model validity, even though it slightly restricts the α values for which our model is valid. We see that even in practical situations where α is smaller than that permitted by our assumptions, the current algorithm performs better than a phase inversion based version able to use $b < 1$.

[10] Even though our choice of b may increase accuracy, we see that in practical situations, the magnitude inversion algorithm generally outperforms the phase inversion algorithm.

4.3.2 Algorithm

Having specified a range over which our model is valid, we may now estimate α from the FFT phase characteristic. If we indeed have a linear frequency chirp, we should see a parabolic phase characteristic in the specified range. If this is the case, the second order difference of the characteristic should be a constant in this range. If this is not the case, the second order difference will be zero or nonconstant. In fact, we may use this fact as a "check" on whether or not our linear chirp model is valid for the smeared peak.

According to our phase model, the constant achieved by this second order differencing operation is

$$\frac{\Delta^2 \angle(Y(k))}{\Delta k^2} \quad \approx \quad \frac{-2\pi^2}{K^2 \alpha}. \tag{116}$$

Since the marginal error in the inverse midpoint approximations will lead to slight but not major deviations from this value, it is prudent to ensure that the deviations are within that allowed by the model (see error bounds above). If this is so, errors may be smoothed out by averaging the values over the frequency range contained in the signal. Thus, we may estimate α as

$$\boxed{\alpha \approx \frac{-2\pi^2}{K^2} \left(\overline{\frac{\Delta^2 \angle(Y(k))}{\Delta k^2}} \right)^{-1}}. \tag{117}$$

where the bar indicates an average over the relevant frequency bins. Our estimate will be accurate within bounds noted above.

5 Examples of Estimating α by Model Inversion

We now apply our algorithms to the problem of estimating α for various types of signals. We begin with linear chirps, including those where the small size of α invalidates the model. Next, we use the same algorithms on monotonic nonlinear frequency function signals, and observe near-optimal results in the least-square sense. Finally, we apply the algorithm to nonmonotonic nonlinear frequency functions.

5.1 Linear Frequency Chirps

We presently apply the algorithm suggested in section 4 to several linear chirp examples where we treat α as unknown initially. In each of these cases, figures 12 through 17, the first subplot shows the magnitude FFT of a signal characterized by some a value noted above the plot. We have also marked the half height point with a dashed line. Without verifying that the corresponding k_{hh} range suggests a sufficiently large α, we estimate an α value by inverting the magnitude expression as described above (and use it to plot our estimate of the instantaneous frequency function in the third subplot). We do not do this verification in order to allow the illustration of "failed attempts" by the algorithm when α (or a) is too small.

In the second subplot, we see the second order difference of the phase, again with the half height region marked. We also show – with dashed vertical lines – bounds for an often more limited region in cases corresponding to $b < 1$ in the phase inversion technique. A horizontal dashed line represents the average phase concavity in this valid range, which we use to backsolve for α via inversion of the phase expression.

In the third subplot, we show the estimated frequency characteristic obtained by backsolving for α using each of the two techniques, along with the original. The phase model is shown with a dashed line and the magnitude model with a dotted line. Each estimated a value is also shown above the plot, next to the actual a value for comparison. We see greater accuracy from the magnitude model in all cases. For these examples and those in the next subsections, we have used a Hann window (as required), $F = 8000$, $N = 201$, and $K = 5 \cdot N$.

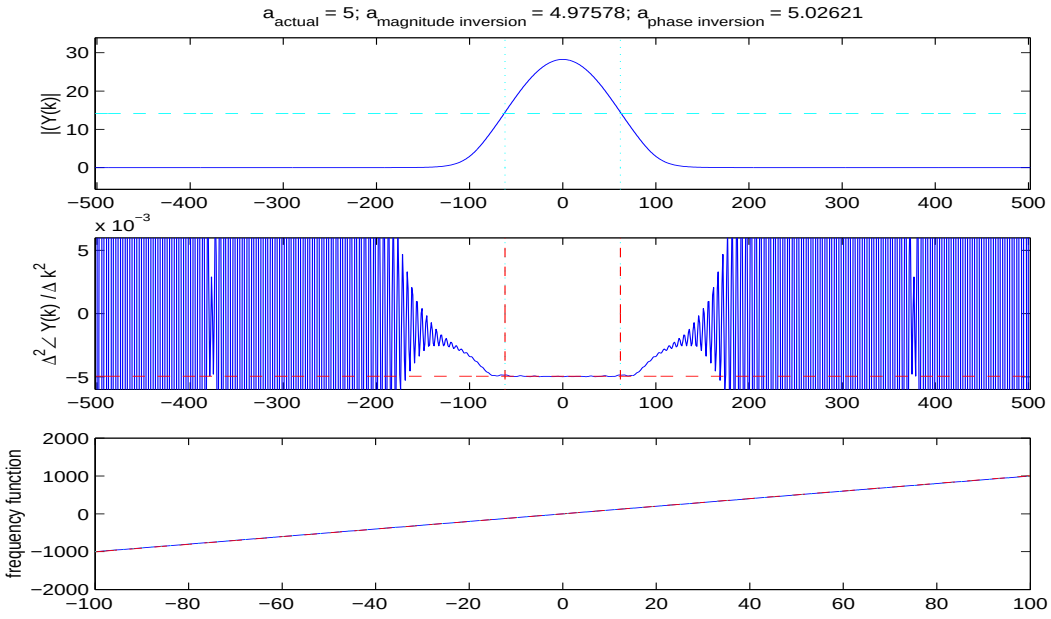

Figure 12: $a = 5$

5.2 Other Monotonic Nonstationary Signals

Now, we apply the algorithm to nonlinear instantaneous frequency functions using only the logic that such functions might be well modeled as quasi-linear. In figures 18 through 21, we show exponential, quadratic, cubic, and logarithmic frequency functions $q(n)$, as well as our system's guess of a parameter α, estimated using inversion techniques identical to those used in the linear frequency chirp case above. To determine how close the algorithm is to optimal for these cases, a least squares fit of an affine function passing through the same detected center frequency is also shown in the third subplot (dot-dash). The corresponding a value, a_{ls}, is shown above the plot with the other estimates. All other plots are presented in the same manner as for the linear frequency case. We make an interesting observation that the phase inversion approximation generally tracks the frequency trajectory more closely than than the magnitude

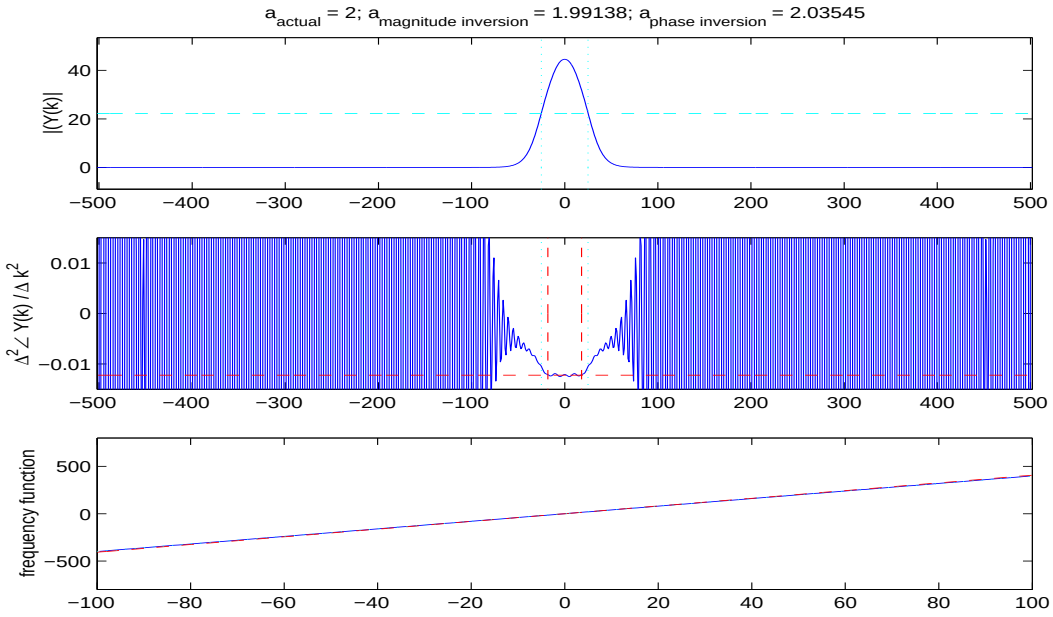

Figure 13: $a = 2$

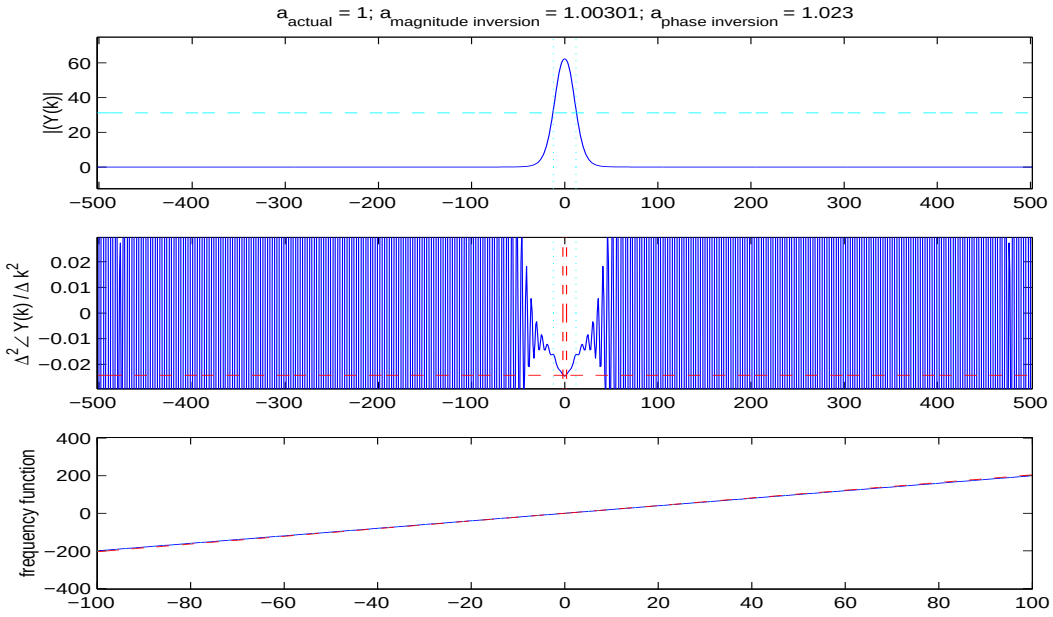

Figure 14: $a = 1$

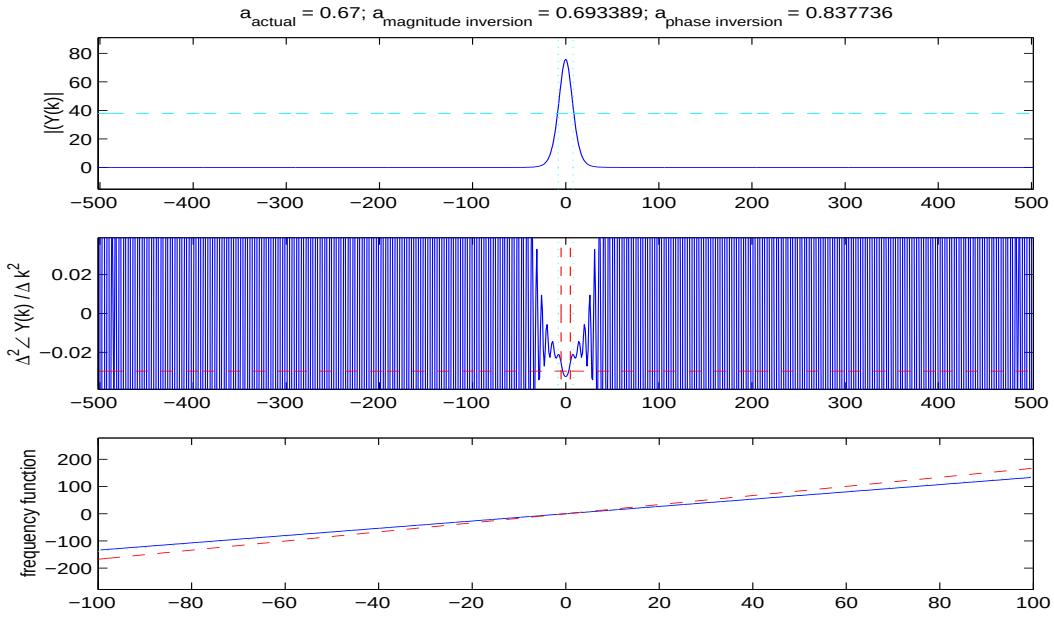

Figure 15: $a = .67$

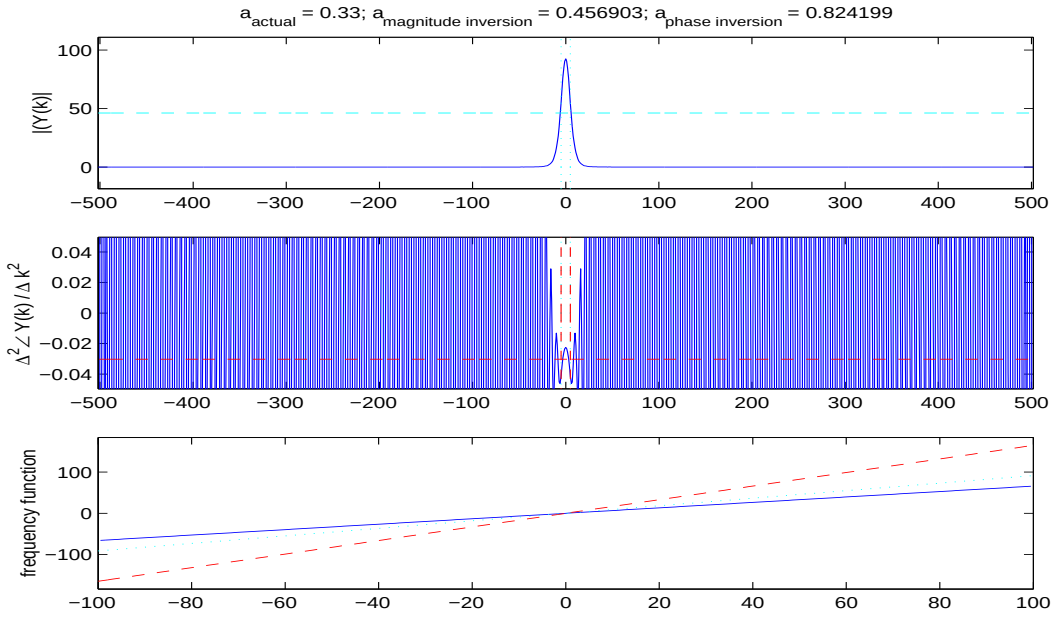

Figure 16: $a = .33$

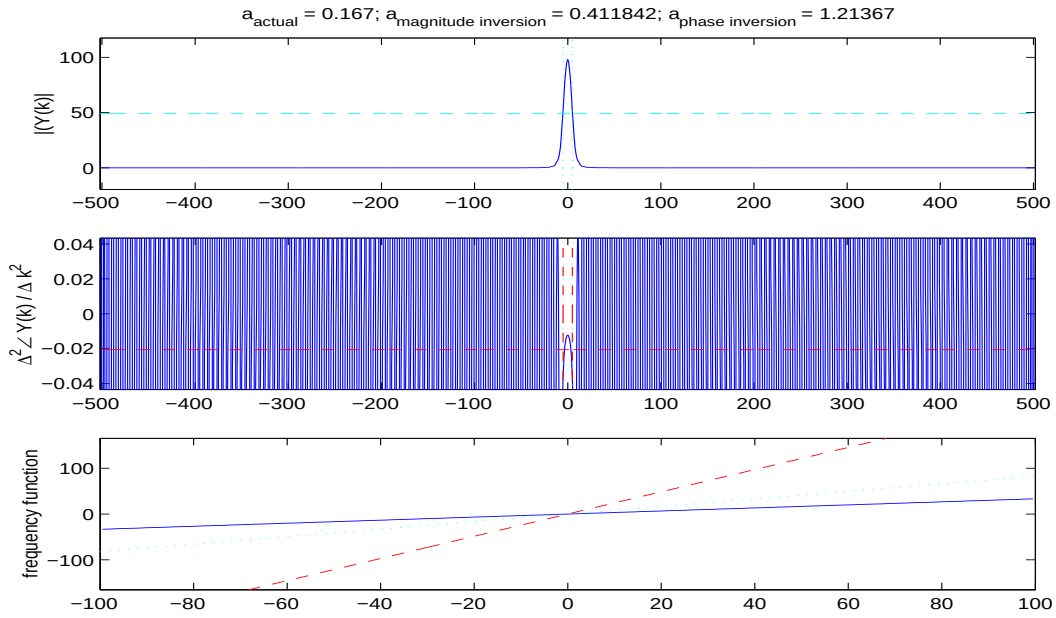

Figure 17: $a = .167$

inversion approximation. In most cases, we see that this approximation is within 3% of a_{ls}, showing that our blind algorithm is, in fact, nearly optimal. In future research, we will explore the underlying cause of this success for the phase inversion approximation.

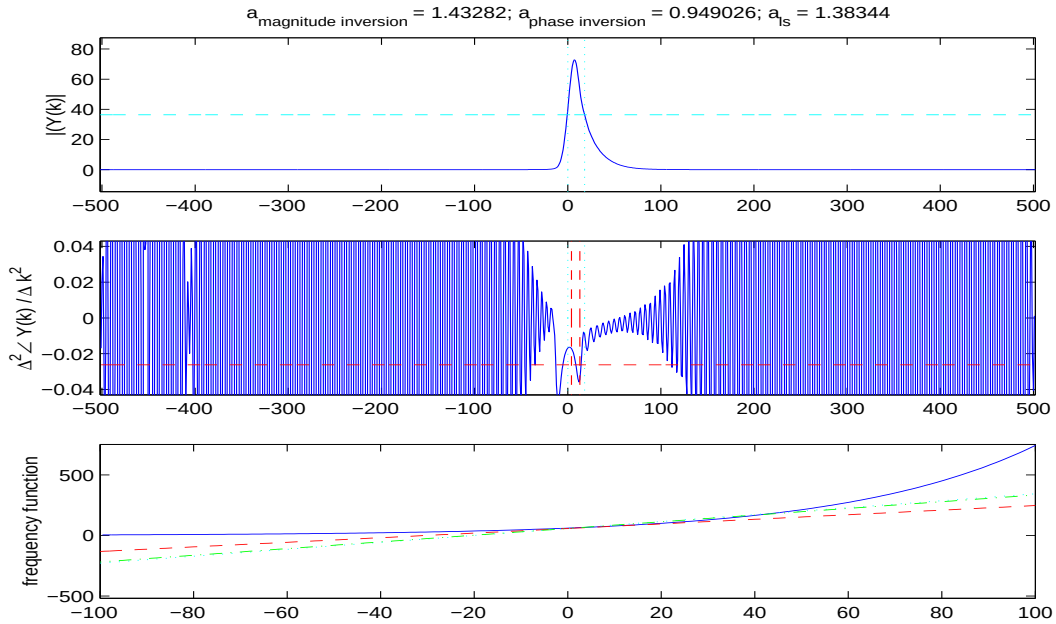

Figure 18: $q(n) = .08 \cdot \exp((n-20)/40)$

5.3 Nonmonotonic Nonstationary Signals

Finally, we apply our algorithm to the case where the instantaneous frequency function is not monotonically increasing or decreasing. Examples of this case are seen in figures 22 through 24. We make the very important observation that the phase inversion model does not in any of these examples show a clear positive or negative characteristic. As a result, the averaging procedure often causes the mean phase concavity to be artificially close zero, so when we

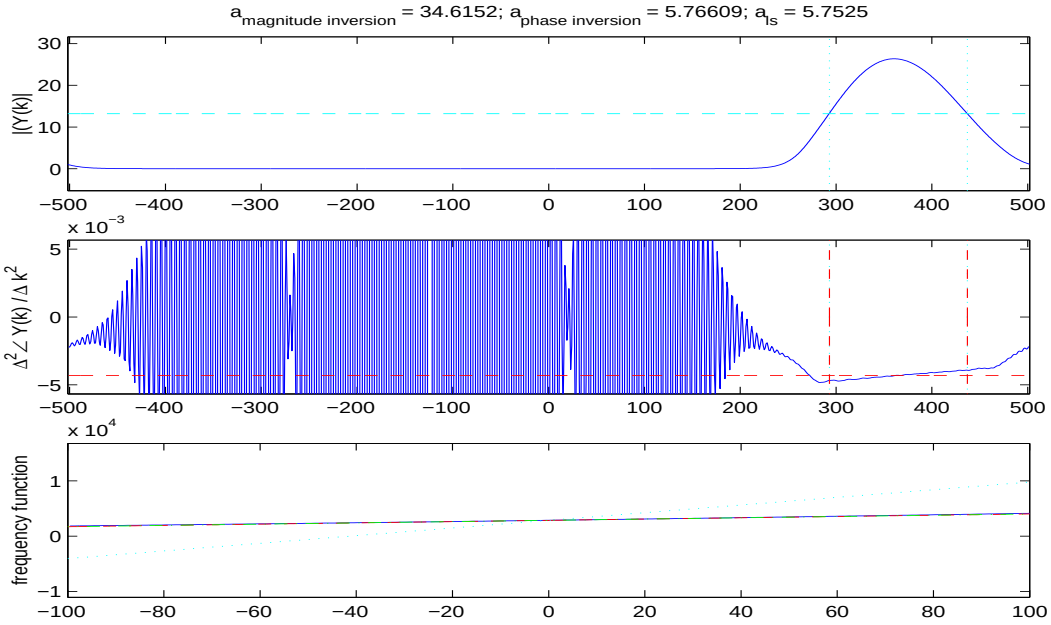

Figure 19: $q(n) = .003 \cdot (n + (K-1)/2)^2$

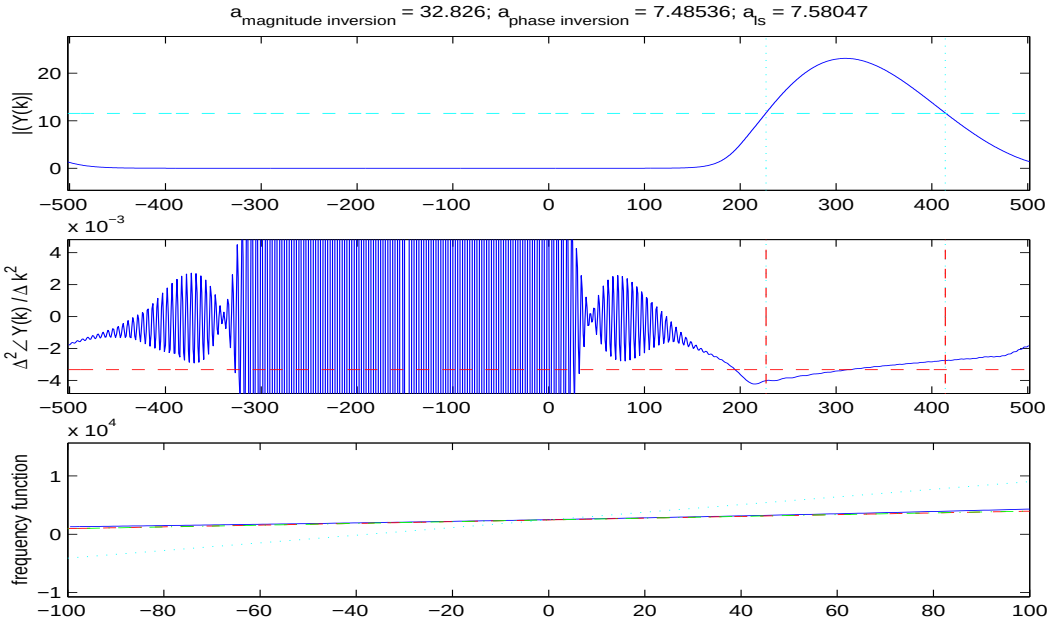

Figure 20: $q(n) = .0025 \cdot (n + (K-1)/2)^3$

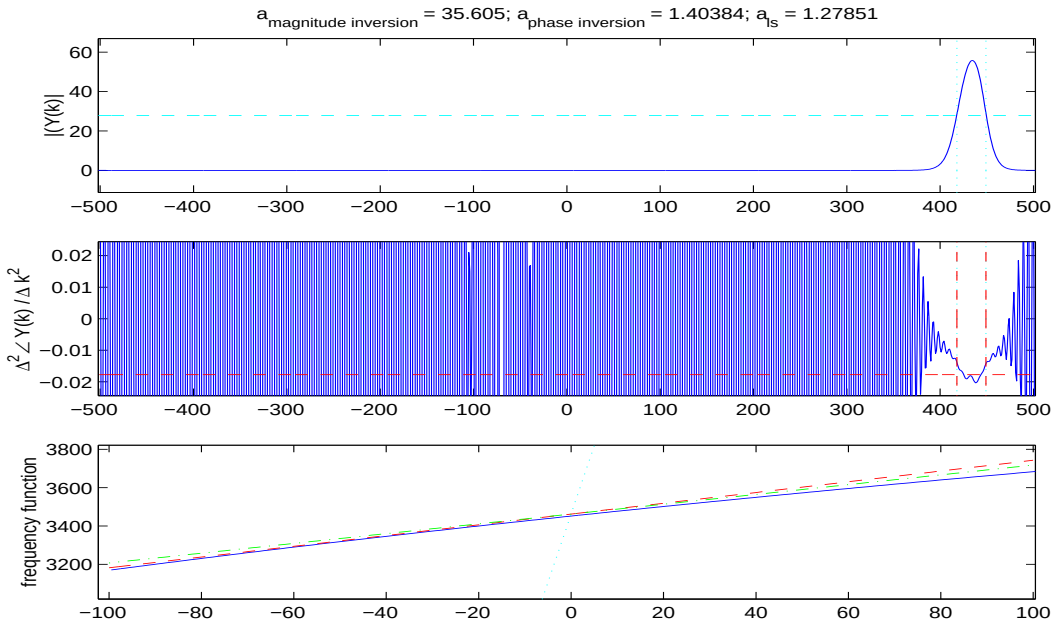

Figure 21: $q(n) = \ln(0.03 \cdot (n + (K-1)/2))$

apply equation 117, we get a very large α estimate. This is of course not in agreement with the magnitude inversion approximation, which generates a much smaller α estimate since the peak width is still narrow. This can be exploited in a chirp detection setting: if the phase concavity is ambiguous (averages to a very small value, causing a very large α estimate) while the peak width is wider than for a quasistationary sinusoid (but still generates a much smaller α than the phase inversion technique), we claim that we do not have a monotonic instantaneous frequency function.

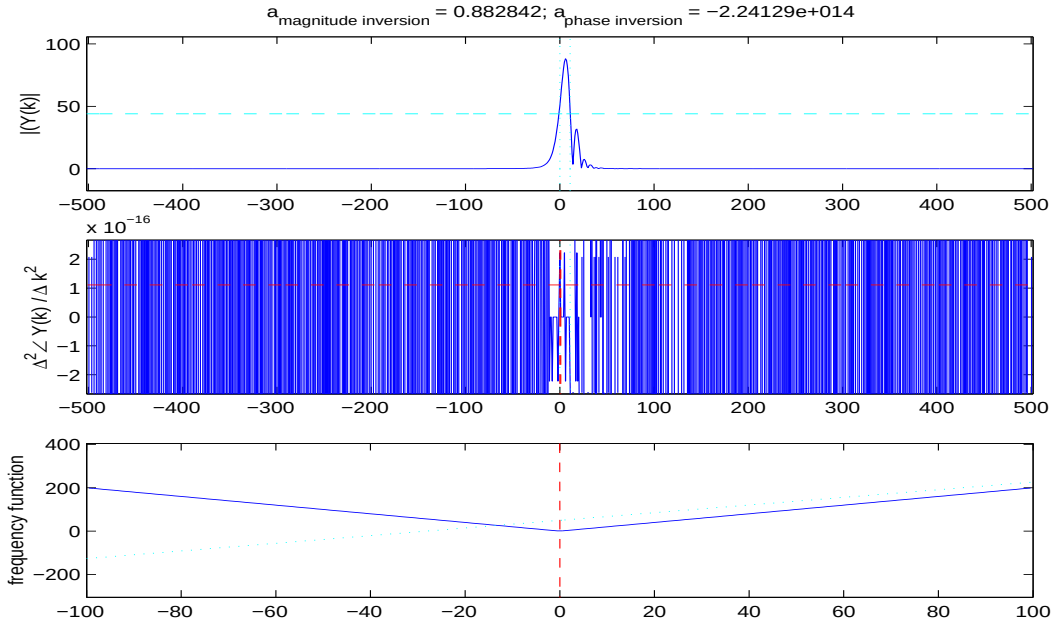

Figure 22: $q(n) = 2 \cdot 2\pi/F|n - 0.5|$

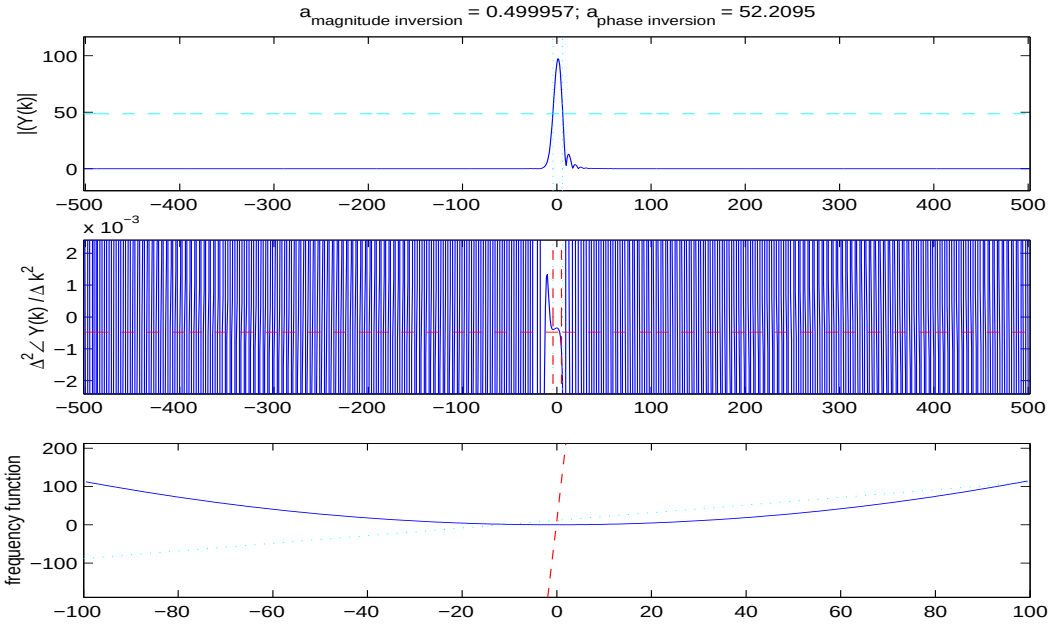

Figure 23: $q(n) = (0.003 \cdot n)^2$

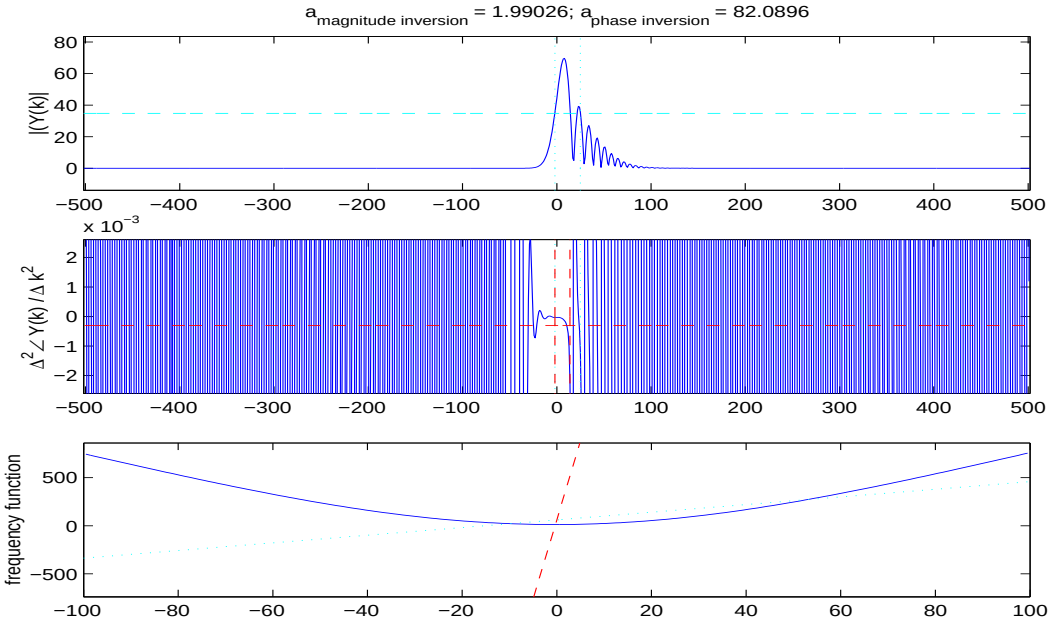

Figure 24: $q(n) = \ln(0.00008 \cdot n^2 + 1.01)$

6 Summary

We presented a model for approximations of the FFT of linear frequency chirps, derived from Fresnel integral analysis. We rigorously showed that when the chirp increases or decreases quickly enough within an analysis frame, our current set of Fresnel assumptions are valid, and the FFT will show parabolic phase. We presented results showing that the model is invertible, allowing calculation of the chirp parameter from the FFT. We showed that the inversion techniques may also be used to make linear approximations to nonlinear frequency trajectories, and to conclude that a frequency trajectory is or is not monotonic.

In appendix A below, we discuss other algorithms that may be used specifically when our α value is too small for the above analysis. These algorithms have already been implemented, and will be fully integrated into a later report.

A Summaries of Other Implemented Algorithms for Future Publication

In this appendix, we present summaries of additional techniques for the chirp parameter estimation problem. Each of these techniques has been implemented by the author, and examples as well as in-depth discussion of each are forthcoming in future reports.

These approaches are still relevant to Fresnel analysis, however, as each relies on Fresnel integrals, but simply uses different approximations of them than those used in the paper above. Specifically, the issue becomes our use of equations 66 and 67 as "valid approximations" of the Fresnel integrals. As mentioned in the writing above, those approximations are not always accurate, depending on α and the frequency bins k considered. Below, we reconsider the approximations used in those equations for

$$\int_{\pm l_1}^{\pm l_2} \cos\left(\frac{\pi}{2}u^2\right) du \tag{118}$$

and

$$\int_{\pm l_1}^{\pm l_2} \sin\left(\frac{\pi}{2}u^2\right) du, \tag{119}$$

where $l_1 = \sqrt{\frac{2\alpha}{\pi}}\left(-\frac{N}{2} - \frac{\pi k}{\alpha K}\right)$ and $l_2 = \sqrt{\frac{2\alpha}{\pi}}\left(\frac{N}{2} - \frac{\pi k}{\alpha K}\right)$.

We show that when α is smaller than permitted above and we choose frequency bins carefully, we may again obtain useful expressions for the real and imaginary parts of $Y_a(k)$, by using what we term the "same sign large limits approximation" and the "small limits approximation."

To compare the performance of these new models to those discussed in the body of the paper (and to Liu's model in appendix B) we conclude this section with comparative plots.

A.1 Same Sign Large Limits Approximation

A.1.1 Rectangular Window

When α is very small, l_1 and l_2 will take on the same sign for almost all frequency bins k, rendering equations 66 and 67 invalid. Fortunately, the large limits approximation may still be used, but while bearing in mind that the limits of integration in those expressions will have the same sign and be close in value to each other. Specifically, we may now state that

$$\int_{\pm l_1}^{\pm l_2} \cos\left(\frac{\pi}{2}u^2\right) du \approx \pm\left(\frac{1}{-l_1\pi}\sin\left(\frac{\pi}{2}(-l_1)^2\right) + \frac{1}{l_2\pi}\sin\left(\frac{\pi}{2}(l_2)^2\right)\right) \tag{120}$$

$$\int_{\pm l_1}^{\pm l_2} \sin\left(\frac{\pi}{2}u^2\right) du \approx \pm\left(-\frac{1}{-l_1\pi}\cos\left(\frac{\pi}{2}(-l_1)^2\right) - \frac{1}{l_2\pi}\cos\left(\frac{\pi}{2}(l_2)^2\right)\right). \tag{121}$$

Continuing algebraically in a similar fashion as before, we apply trigonometric identities and obtain

$$\Re Y_a(k) \approx \frac{-1}{l_2\pi}\cos\left(i\left(\frac{\pi}{2} - \phi + \frac{\pi}{2}l_2^2\right)\right) + \frac{1}{l_1\pi}\cos\left(i\left(\frac{\pi}{2} - \phi + \frac{\pi}{2}l_1^2\right)\right) \tag{122}$$

$$\Im Y_a(k) \approx \frac{-1}{l_2\pi}\sin\left(i\left(\frac{\pi}{2} - \phi + \frac{\pi}{2}l_2^2\right)\right) + \frac{1}{l_1\pi}\sin\left(i\left(\frac{\pi}{2} - \phi + \frac{\pi}{2}l_1^2\right)\right). \tag{123}$$

We make note that this only applies when both l_1 and l_2 have magnitude much greater than one, and have the same sign. This will occur only when α is very small and k is at least slightly greater than zero. At $k = 0$, the large limits approximation is simply not valid.[11]

[11] The small limits approximation applies there. This is covered in the next subsection.

In order to extract the parameter α from a model based on equations 122 and 123, we must make a critical analysis of the situation: a closed form expression for the phase cannot be obtained unless the arguments of the sinusoids in these equations are identical. It can be shown that this in fact occurs when we choose $k = \frac{K}{N}p$ where p are nonzero integers less than $\frac{N}{2}$. Doing so shows that, for odd p,

$$\angle Y_a(k) = \frac{\alpha N^2}{4} - \frac{\pi}{2}, \tag{124}$$

and that for even p,

$$\angle Y_a(k) = \frac{\alpha N^2}{4} + \frac{\pi}{2}, \tag{125}$$

which we may solve for α to obtain

$$\boxed{\alpha \approx \frac{4}{N^2}\left(\angle Y\left(\frac{K}{N}p\right) + \frac{\pi}{2}\right)} \tag{126}$$

for odd p and

$$\boxed{\alpha \approx \frac{4}{N^2}\left(\angle Y\left(\frac{K}{N}p\right) - \frac{\pi}{2}\right)} \tag{127}$$

for even p.

Thus, to estimate α, we simply substitute values of the angle of the FFT at $k = \frac{K}{N}p$ into the appropriate expression above. We note that all exponential and sinusoidal arguments take on values between 0 and 2π in this analysis.

A.1.2 Hann Window

We recall that using a time domain Hann window may be viewed as a weighted averaging operation in the frequency domain. This actually presents more of a problem than a convenience for the same sign large limits approximation, because the expressions obtained above are *not* valid for $k = 0$, or for k near zero, with the exact k depending on α. Thus, making conclusions about α by inspecting $Y_a^{Hann}\left(\frac{K}{N}\right)$ is impossible, because this value of Y relies on $Y_a^{Rect}(0)$.

One way around this problem is to inspect $Y_a^{Hann}\left(2\frac{K}{N}\right)$ instead, but in practice this is not always possible. This is because $2\frac{K}{N}$ is nearly a local minimum, and is thus easily obscured by other interfering peaks.

A somewhat better solution is to consider $Y_a^{Hann}\left(2.5\frac{K}{N}\right)$. In the required Y bins there, the large limits same sign approximations are still valid. This is still problematic, however, since they are still not near to the maximum value of the peak, and thus are subject to interference from other sinusoids. This idea might at first seem mathematically objectionable as well, since the arguments of the sinusoids will no longer be equal. We observe, however, that the arguments will differ from each other by exactly π, meaning that vector addition requires their weighted sum lie on the same line, with the same phase. As a result, the phase will be:

$$\angle Y_a\left(2.5\frac{K}{N}\right) = \frac{\alpha N^2}{4} - \pi, \tag{128}$$

which we may solve for α to obtain

$$\boxed{\alpha \approx \frac{4}{N^2}\left(\angle Y\left(2.5\frac{K}{N}\right) + \pi\right).} \tag{129}$$

A.2 Small Limits Approximation

A.2.1 Rectangular Window

We noted in the previous subsection that the large limits same sign approximation is not usable for $k = 0$. This was, in fact, because when $k = 0$ and α is small, l_1 and l_2 become too small to use the large limits approximation in any form. Fortunately, we may consider alternate functions that well approximate the Fresnel cosine and sine integrals for $|u| < 1$. Specifically, the author determined empirically that equations 66 and 67 are well-modeled as

$$\int_{\pm l_1}^{\pm l_2} \cos\left(\frac{\pi}{2}u^2\right) du \approx l_2 - l_1 \tag{130}$$

$$\int_{\pm l_1}^{\pm l_2} \sin\left(\frac{\pi}{2}u^2\right) du \approx \frac{l_2^3}{2} - \frac{l_1^3}{2}. \tag{131}$$

Continuing algebraically as before and considering l_1 and 1_2 when $k = 0$, we obtain:

$$\Re Y_a(0) \approx N \tag{132}$$

$$\Im Y_a(0) \approx \frac{\alpha N^3}{4\pi}. \tag{133}$$

The imaginary expression may be solved for α to get

$$\boxed{\alpha \approx \frac{\Im Y_a^{Rect}(0) \cdot 4\pi}{N^3}.} \tag{134}$$

A.2.2 Hann Window

As noted in the previous subsection, we may think of applying the time domain Hann window as creating a weighted frequency domain sum. In the current situation, this again can become problematic. Since we are using the small limits approximation to obtain $Y(0)$, the Hann window requires us to consider $Y_a^{Rect}\left(-\frac{K}{N}\right)$ and $Y_a^{Rect}\left(\frac{K}{N}\right)$ as well. Mathematically, this presents a difficulty, since the small limits approximation is *not* valid for $Y_a^{Rect}\left(\pm\frac{K}{N}\right)$. We can still use the large limits approximation to consider those values. This, however, does not lead to an elegant or invertible expression for α. Fortunately, it can be shown that $Y_a\left(\pm\frac{K}{N}\right) \approx 0$. Intuitively, this makes sense, because as α becomes very small, the "chirp" signal becomes a quasistationary sinusoid, and the FFT converges to the window transform of the signal which is identically zero at $\pm\frac{K}{N}$. Applying this idea, we have that

$$\boxed{\alpha \approx 2 \cdot \frac{\Im Y_a^{Hann}(0) \cdot 4\pi}{N^3}.} \tag{135}$$

A.3 Comparative Plots

For each of several sets of example signals with noted signal-to-noise ratios, we see the rectangular window models in the first subplot and the Hann window models in the second subplot. As expected, the magnitude inversion model discussed above reaches an asymptotic value corresponding to the width of the window transform. We also see the empirical effect of the minimum α requirements mentioned repeatedly above.

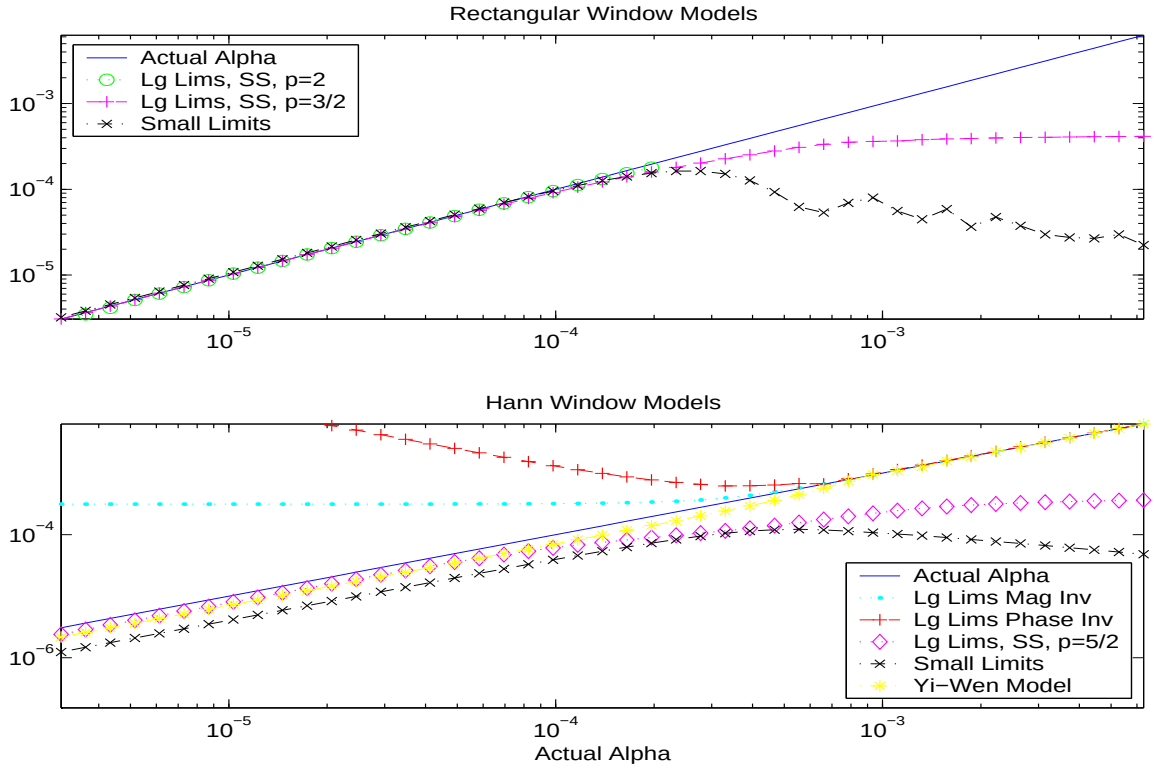

Figure 25: SNR = 40 db

B Yi-Wen Liu's Model

Liu has recently considered the continuous time linear frequency chirp case. He has presented a result showing that the second derivative of the Fourier transform of such a signal with respect to frequency yields a convenient expression

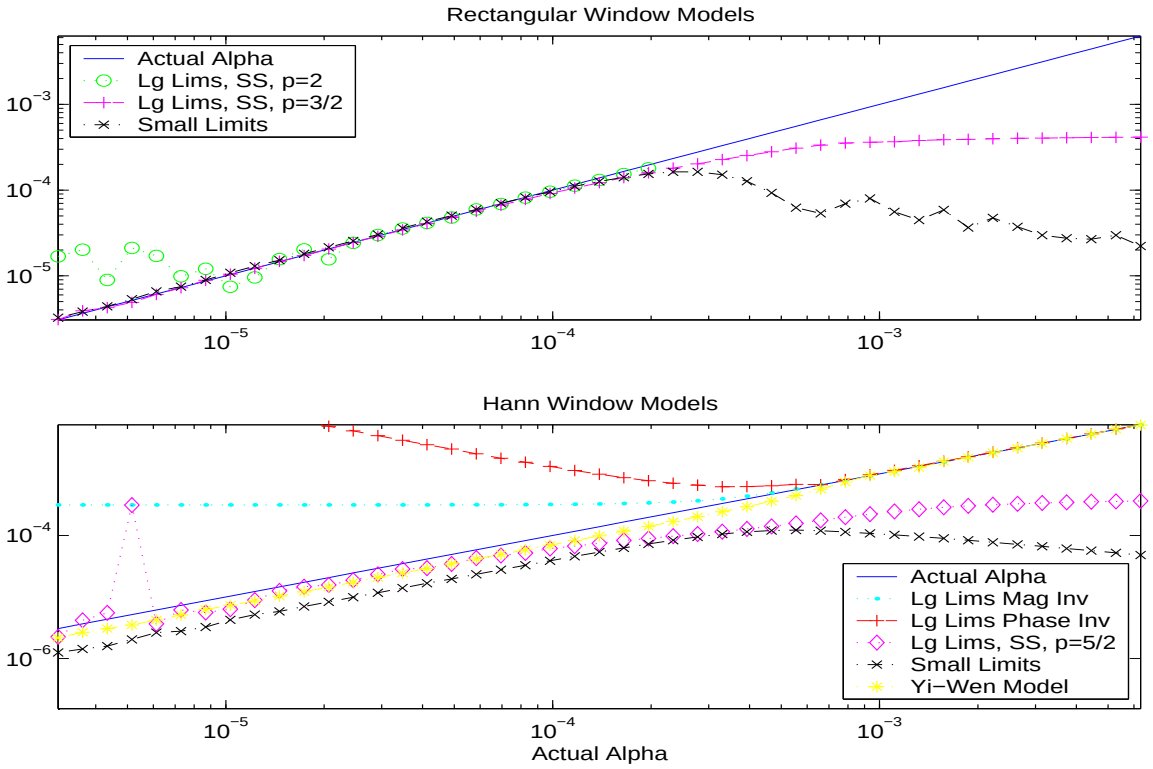

Figure 26: SNR = 20 db

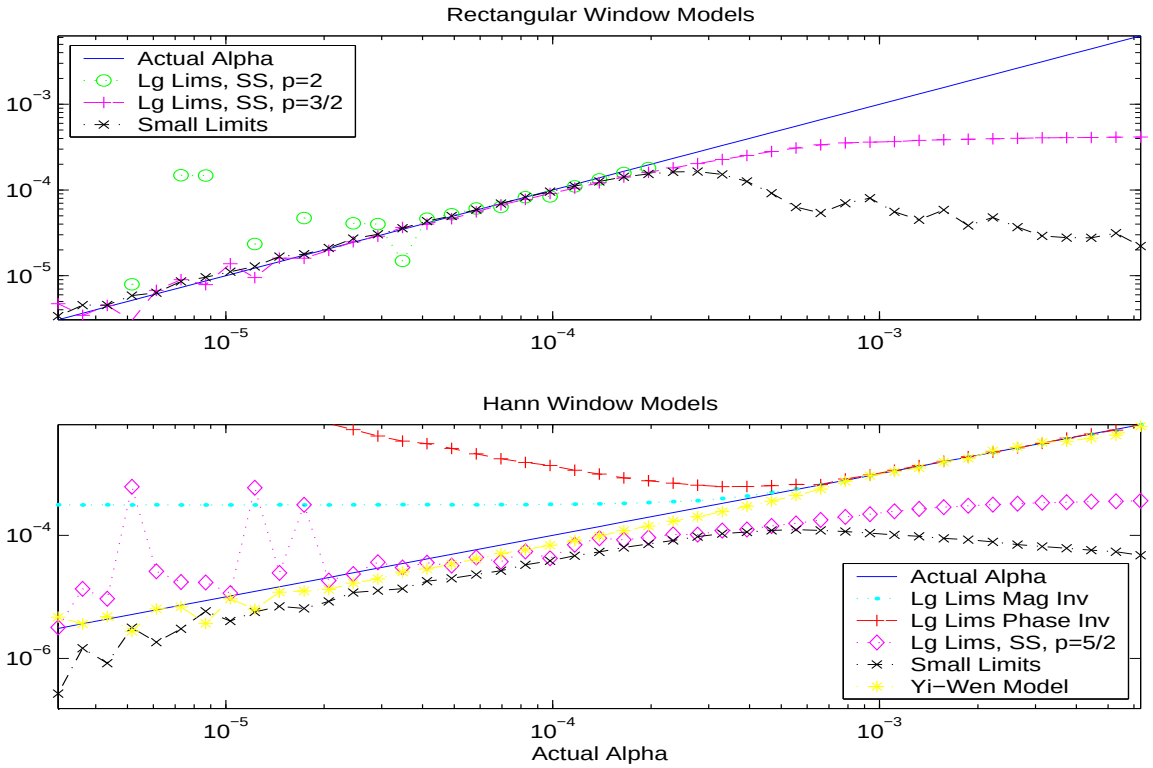

Figure 27: SNR = 10 db

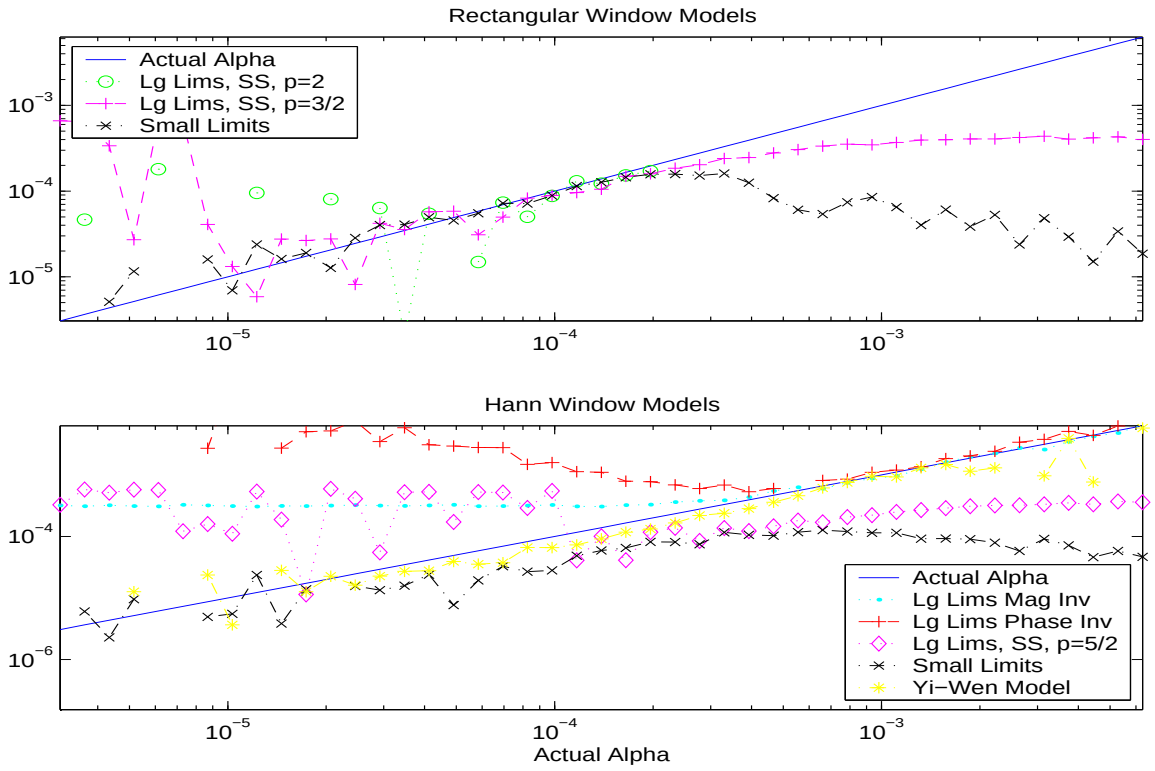

Figure 28: SNR = 0 db

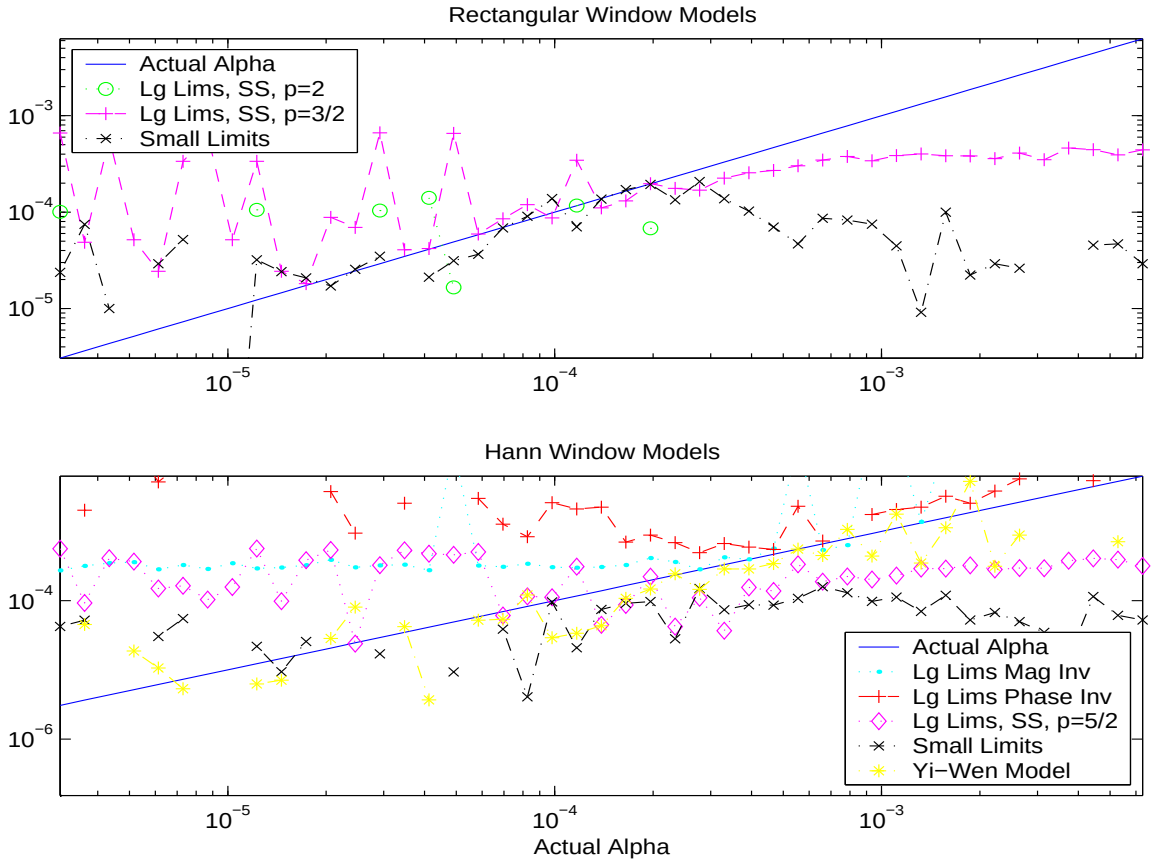

Figure 29: SNR = -5 db

in terms of α. Specifically, at the continuous frequency corresponding to DC ($\omega = 0$), Liu finds that

$$\frac{d^2 Y_W^{\text{Hann}}(\omega)}{d\omega^2}\Big|_{\omega=0} = \frac{-j}{2\alpha}(Y_W^{\text{Hann}}(0)). \tag{136}$$

We now extend Liu's result to discrete time. Equation 136 thus becomes:

$$\left(\frac{K}{2\pi}\right)^2 \frac{\Delta^2 Y^{\text{Hann}}(k)}{\Delta k^2}\Big|_{k=0} = \frac{-j}{2\alpha}(Y^{\text{Hann}}(0)). \tag{137}$$

where we note that second order differencing operation with respect to frequency bin k must be normalized by twice multiplying by $\frac{K}{2\pi}$. This expression may be solved for alpha to obtain:

$$\boxed{\alpha \approx \frac{-jY^{\text{Hann}}(0)}{2}\left(\left(\frac{K}{2\pi}\right)^2 \frac{\Delta^2 Y^{\text{Hann}}(k)}{\Delta k^2}\Big|_{k=0}\right)^{-1}.} \tag{138}$$

C Error Propagation Analysis

In sections 4.3 and 4.2, we alluded to the fact that error in the real and imaginary parts of the FFT of our chirp signal propagates differently in calculations of the magnitude and phase of the FFT. We consider error in each of these calculations in separate subsections below.

C.1 Large Limits Approximation Error Propagation in Magnitude Estimate

To obtain the magnitude estimate from the real and imaginary estimates, we must perform:

$$|Y_a(k)| = \sqrt{(\Re Y_a(k))^2 + (\Im Y_a(k))^2}, \tag{139}$$

which includes two squaring operations, a sum operation, and a square root operation. To make our analysis cleaner, we define:

$$A = \Re Y_a(k) \qquad B = \Im Y_a(k) \tag{140}$$

$$X = A^2 \qquad Y = B^2 \tag{141}$$

$$Z = X + Y \qquad |Y_a(k)| = \sqrt{Z} \tag{142}$$

and denote the error in any variable V as ΔV. The table below shows how each variable manifests error as a result of error in variables of which it is a function. Rigorous justification of the error propagation shown is given in [7].

Relating Function	Error Propagated
$X = A^2$	$\Delta X = 2A\Delta A$
$Y = B^2$	$\Delta Y = 2B\Delta B$
$Z = X + Y$	$\Delta Z = \sqrt{(\Delta X)^2 + (\Delta Y)^2}$
$\lvert Y_a(k)\rvert = \sqrt{Z}$	$\Delta\lvert Y_a(k)\rvert = \frac{1}{2}Z^{\frac{-1}{2}}\Delta Z$

Making appropriate substitutions, we thus get

$$\Delta|Y_a(k)| = \frac{\sqrt{(A\Delta A)^2 + (B\Delta B)^2}}{\sqrt{A^2 + B^2}} = \frac{\sqrt{(\Re Y_a(k)\Delta\Re Y_a(k))^2 + (\Im Y_a(k)\Delta\Im Y_a(k))^2}}{|Y_a(k)|} \tag{143}$$

C.2 Large Limits Approximation Error Propagation in Phase Estimate

We now apply a similar analysis to the phase case. We recall that in section 4.3 we base our estimate of α on the second order difference of the phase of $Y(k)$. Stating this in terms of the real and imaginary parts thereof, we have:

$$\frac{\Delta^2 \angle Y(k)}{\Delta k^2} = \frac{\Delta^2}{\Delta k^2}\arctan\left(\frac{\Im Y(k)}{\Re Y(k)}\right). \tag{144}$$

Proceeding as above, we make the notation cleaner in our error propagation analysis by defining

$$A(k) = \Re Y_a(k) \qquad B(k) = \Im Y_a(k) \tag{145}$$

$$U = \frac{B}{A} \qquad T = \arctan(U) \tag{146}$$

$$S = T(k) - T(k-1) \qquad \frac{\Delta^2 \angle Y(k)}{\Delta k^2} = S(k) - S(k-1) \tag{147}$$

We again create an error manifestation table below. We make an important exception to the general treatment of error propagation in the case of propagating error from T to S, and from S to the final result. Instead of treating these differencing operations as the subtraction of independent errors – which results in propagating the error as a Euclidean distance (as in the addition in the previous subsection) – we acknowledge that the neighboring errors are highly correlated, and thus their combination is best modeled as a simple subtraction. This is reflected in the table below.

Relating Function	Error Propagated
$U = \frac{B(k)}{A(k)}$	$\Delta U = \sqrt{B^2 \Delta A^2 + A^2 \Delta B^2}$
$T = \arctan(U)$	$\Delta T = \frac{\Delta U}{1+U^2} \leq \Delta U$
$S = T(k) - T(k-1)$	$\Delta S = \Delta T(k) - \Delta T(k-1)$
$\frac{\Delta^2 \angle Y(k)}{\Delta k^2} = S(k) - S(k-1)$	$\Delta \frac{\Delta^2 \angle Y(k)}{\Delta k^2} = \Delta S(k) - \Delta S(k-1)$

Making appropriate substitutions, we obtain

$$\begin{aligned}
\Delta \frac{\Delta^2 \angle Y(k)}{\Delta k^2} &= \Delta T(k) - 2\Delta T(k-1) + \Delta T(k-2) && (148)\\
&= \sqrt{(B(k)\Delta A(k))^2 + (A(k)\Delta B(k))^2} \\
&- 2\sqrt{(B(k-1)\Delta A(k-1))^2 + (A(k-1)\Delta B(k-1))^2} && (149)\\
&+ \sqrt{(B(k-2)\Delta A(k-2))^2 + (A(k-2)\Delta B(k-2))^2} \\
&= \sqrt{(\Im Y(k)\Delta \Re Y(k))^2 + (\Re Y(k)\Delta \Im Y(k))^2} \\
&- 2\sqrt{(\Im Y(k-1)\Delta \Re Y(k-1))^2 + (\Re Y(k-1)\Delta \Im Y(k-1))^2} && (150)\\
&+ \sqrt{(\Im Y(k-2)\Delta \Re Y(k-2))^2 + (\Re Y(k-2)\Delta \Im Y(k-2))^2}.
\end{aligned}$$

It can be seen by inspection that in some cases, the error can be nearly zero, while in others, it may be double the first term. This depends on the correlation of the real part with the error in the imaginary part and vice versa. These correlations vary rapidly with k, as can be seen in the example plotted earlier (figure 10) where the error appeared unstable. The rapid variation does not appear to suggest an invertible error model, and as a result is in general more damaging to an estimation algorithm. The magnitude of the error in the worst cases is also problematic, as we note that the error here is not divided by $|Y(k)|$ as it was in the magnitude case. Thus, the error propagation in implementation here is more problematic than that for the magnitude case in the previous subsection. This fact is also reflected somewhat in the accuracy obtained in estimating α using each model.

D Appendix: Non-Validity of the Infinite Fresnel Integral Limits Approximation for the Rectangle Window

D.1 Definition of Approximation

Something not covered above was the effect of using the infinite limits approximation directly, while still using the rectangular window. Herein, we rigorously show why this is not a valid approach. We begin our pursuit of this doomed idea by stating the assumption:

$$\pm\sqrt{\frac{2\alpha}{\pi}}\left(-\frac{N}{2} - \frac{\pi k}{\alpha K}\right) \approx \mp\infty \qquad \pm\sqrt{\frac{2\alpha}{\pi}}\left(\frac{N}{2} - \frac{\pi k}{\alpha K}\right) \approx \pm\infty. \tag{151}$$

This approximation is a much stronger one than the large limits approximation, and allows a greatly simplified expression for the real and imaginary parts of $Y_a(k)$. Here, we consider why this is not valid for the rectangle window case. Though our result is discouraging, we recall that the infinite limits approximation may in fact be simulated by using a different windowing function, as has been covered earlier.

To explore the validity of the infinite limits approximation for the rectangle window case, we will compare this approximation to that made above (the large limits approximation). Since we know the large limits approximation is very accurate (to within 2.3% for $c = 2$) we will consider the error introduced by the infinite limits approximation *relative* to the large limits approximation, and judge its validity accordingly.

Presently, we compare the large limits approximation

$$\begin{aligned}
\int_{\pm l_1}^{\pm l_2} \cos\left(\frac{\pi}{2}u^2\right) du &\approx \pm\left(1 + \frac{1}{-l_1\pi}\sin\left(\frac{\pi}{2}(-l_1)^2\right) + \frac{1}{l_2\pi}\sin\left(\frac{\pi}{2}(l_2)^2\right)\right) && (152)\\
\int_{\pm l_1}^{\pm l_2} \sin\left(\frac{\pi}{2}u^2\right) du &\approx \pm\left(1 - \frac{1}{-l_1\pi}\cos\left(\frac{\pi}{2}(-l_1)^2\right) - \frac{1}{l_2\pi}\cos\left(\frac{\pi}{2}(l_2)^2\right)\right), && (153)
\end{aligned}$$

and the infinite limits approximation

$$\int_{\pm l_1}^{\pm l_2} \cos\left(\frac{\pi}{2}u^2\right) du \approx \pm\int_{-\infty}^{\infty} \cos\left(\frac{\pi}{2}u^2\right) du = \pm 1 \tag{154}$$

$$\int_{\pm l_1}^{\pm l_2} \sin\left(\frac{\pi}{2}u^2\right) du \approx \pm\int_{-\infty}^{\infty} \sin\left(\frac{\pi}{2}u^2\right) du = \pm 1. \tag{155}$$

and see that the infinite limits approximation allows us to drop the sinusoidal terms we included in the large limits approximation.

D.2 Test of the Infinite Limits Approximation for the Rectangle Window

Since each dropped term is amplitude modulated by $\frac{1}{\pi(-l_1)}$ or $\frac{1}{\pi(l_2)}$, dropping the terms at worst throws off our approximation by these amounts. Stated formally, the error introduced by the assumptions in equations 154 and 155 is bounded by

$$|e_\infty| \leq \frac{1}{-l_1\pi} + \frac{1}{l_2\pi} \tag{156}$$

Taking a cue from other analysis herein, we may express our desire that the error introduced is much less than 1 as $|e_\infty| < 1 \cdot q$, where q is a constant less than 1. Simplifying, we have

$$q \cdot 1 \geq \frac{1}{-l_1\pi} + \frac{1}{l_2\pi} \tag{157}$$

$$= \left(\pi\sqrt{\frac{2\alpha}{\pi}}\left(-\frac{N}{2} - \frac{\pi k}{\alpha K}\right)\right)^{-1} + \left(\pi\sqrt{\frac{2\alpha}{\pi}}\left(\frac{N}{2} - \frac{\pi k}{\alpha K}\right)\right)^{-1} \tag{158}$$

$$= \frac{N\sqrt{2\alpha\pi}}{\pi 2\alpha\left(\frac{N^2}{4} - \frac{\pi^2 k^2}{\alpha^2 K^2}\right)} = \left(\sqrt{2\alpha\pi}\left(\frac{N}{4} - \frac{\pi^2 k^2}{\alpha N K^2}\right)\right)^{-1}. \tag{159}$$

We observe that the above expression gives the error incurred q as a function of k. Inspecting this expression, we see that q takes its minimal values when $k = 0$ or when $|k| \gg \frac{N}{4}$. Since k being large violates other necessary assumptions, we consider the $k = 0$ case and solve for $q_{\min}$:

$$q_{\min} = \frac{4}{N}\sqrt{\frac{1}{2\pi\alpha}}. \tag{160}$$

We also wish to know the frequency range over which our assumption is approximately valid. We may solve equation 159 for k in terms of q to see that we require

$$k < \frac{K}{\pi}\sqrt{\frac{\alpha N^2}{4} - \frac{N}{q}\sqrt{\frac{\alpha}{2\pi}}}. \tag{161}$$

Inspecting equation 160 and recalling that $q = 1$ represents the case where the error bound magnitude equals that of the good data, we see that the maximum error resulting from the infinity approximation can indeed be significant, and we find the infinite limits approximation invalid for the rectangle window. Instead, we must use the large limits approximation. As mentioned above, inspection of the corresponding expressions (equations 68 and 69) shows that obtaining a closed form expression for the phase is all but impossible.

References

[1] Lawrence S. Husch Mathematics Department, University of Tennessee, Knoxville. http://archives.math.utk.edu/visual.calculus/4/approx.2/

[2] Yi-Wen Liu. Proof of Concave Phase in Continuous Time Chirp Signals. Stanford University Research Update, 2002.

[3] Aaron S. Master. Sinusoidal Modeling Parameter Estimation via a Dynamic Channel Vocoder Model. Proceedings of ICASSP 2002.

[4] R. J. McAulay and T. F. Quatieri. Speech Analysis-Synthesis Based on a Sinusoidal Representation Lincoln Laboratory Tech Report 693. MIT, 1985.

[5] Julius O. Smith and Xavier Serra PARSHL: A Program for the Analysis/Synthesis of Inharmonic Sounds Based on a Sinusoidal Representation Int Computer Music Conf, 1987

[6] Eric Weisstein. Fresnel Integrals - from MathWorld. http://mathworld.wolfram.com/FresnelIntegrals.html

[7] Frank Wolfs. Error Analysis. http://teacher.nsrl.rochester.edu/phy_labs/AppendixB/AppendixB.html